Characterising the magnetic and plasma environment upstream of Ganymede

A. Santos[1], N. Achilleos[1], D. Millas[2,1], W. Dunn[1], P. Guio[1,3], C. S. Arridge[4]

[1]Department of Physics and Astronomy, University College London, London, UK
[2]Royal Observatory of Belgium, Solar-Terrestrial Centre of Excellence-SIDC, Ringlaan -3- Avenue Circulaire, 1180, Brussels, Belgium
[3]Department of Physics and Technology, Arctic University of Norway, Tromsø, Norway
[4]Department of Physics, Lancaster University, Bailrigg, Lancaster, LA1 4YB, UK

Key Points:

- Strict constraints on magnetospheric field and plasma configuration can be inferred from magnetic field observations alone
- Jupiter's rotation and the position of Ganymede relative to the plasma sheet drive the magnetic and plasma environments surrounding the moon
- Magnetic and hot plasma pressures assume the dominant roles in dictating the plasma environment near Ganymede

Corresponding author: Alexandre Santos, `alexandre.santos.21@ucl.ac.uk`

Abstract

We present an application of the latest UCL-AGA magnetodisc model (MDISC) to the study of the magnetic and plasma conditions in the near-Ganymede space. By doing this, we provide a comparison with measurements from Juno's most recent flyby of the Jovian moon, perijove 34 (PJ34). We find good agreement between the model results and the magnetometer data, pointing towards a hot plasma index value $K_h = (2.719 \pm 0.024) \times 10^7\,\mathrm{Pa\,m\,T^{-1}}$ and an effective magnetodisc radius $r_{\max} = (79.5 \pm 1.1)$ Jupiter radii for the Jovian magnetosphere, for the duration of the trajectory, suggesting a configuration with middling levels of expansion. We also predict the plasma conditions observed by Juno during the same flight-path, as well as the typical conditions over the orbit of Ganymede, with the magnetic and hot plasma pressures assuming dominant roles. Finally, these results are compared with functional fits of a compilation of Galileo flyby data obtained in the vicinity of Ganymede's orbit, suggesting Juno experienced somewhat similar conditions, despite a systematic overestimation in magnetic field intensity in the near-Ganymede space.

Plain Language Summary

Being the largest moon in the Solar system and the only one with its own magnetic field, Ganymede presents a unique target for magnetospheric interaction studies. Although much weaker than the Jovian magnetic field surrounding it, Ganymede's field is strong enough to carve a small region in space, called a magnetosphere, which is itself contained within Jupiter's own magnetosphere. The interplay between these two structures gives rise to numerous phenomena that can affect the near-Ganymede environment. There is also evidence for an additional inductive contribution resulting from the interaction of Jupiter's time varying magnetic field and a possible subsurface ocean. By understanding how the different field contributions affect the overarching environment around Ganymede, we can extract valuable information about the moon's atmosphere, internal composition and its relation with the Jovian environment. In this study we compare our model's predictions with data gathered by Juno during one of its orbits around Jupiter, which also included a Ganymede flyby, showing good agreement between the two. We then predict the plasma conditions the spacecraft encountered during the same trajectory, as well as over Ganymede's orbit, highlighting the main pressure contributions and how these vary according to the rotational phase of Jupiter's magnetic pole.

1 Introduction

Jupiter's magnetosphere constitutes one of the most vast and complex environments in the Solar system, second only to the Sun's own heliosphere. Alongside Saturn, Jupiter's magnetosphere possesses several characteristics that differentiates it from others, such as its enormous size that is supported by an intense internal magnetic field, with an equatorial strength of close to 420 000 nT, and the planet's short rotational period of < 10 hours, which in turn produces large centrifugal forces on the plasma that surrounds the planet. This high volume of plasma originates mainly through intense volcanic activity on Io, one of Jupiter's moons, and plays a vital part in shaping the overarching structure of the Jovian magnetosphere. Due to the planet's rapid rotation, the plasma is confined to a disc-like structure, whose azimuthal current density causes a radial stretching of the magnetic field lines along the magnetic equator, forming the structure known as the *magnetodisc*. This idea was first proposed by Gledhill (1967) and constitutes a significant departure from the dipole description used to model other planetary magnetosphere, such as that of the Earth. The persistent presence of the Jovian magnetodisc has been confirmed through measurements taken by multiple spacecraft, such as Pioneer 10 (Simpson et al., 1974), Voyager 1 (Connerney et al., 1982), Galileo (Kivelson et al., 1997) and, most recently, Juno (Connerney et al., 2017). The continuous interaction be-

tween the Jovian magnetosphere and the solar wind, as well as other internal drivers, also makes it a highly dynamic system.

Ganymede, another of Jupiter's moons, and the largest moon in the Solar system, is also the only one that possesses its own internal magnetic field (Kivelson et al., 2002), which is thought to be dipolar in nature and produced by the dynamo action at the moon's molten core. Having an equatorial field strength of 719 nT, roughly seven times the intensity of the ambient Jovian field at Ganymede's orbital radius (Kaweeyanun et al., 2020), Ganymede's internal field is able to carve a small magnetosphere deep within Jupiter's. Due to Ganymede orbiting the planet close to the Jovigraphic (rotational) equatorial plane and at a distance of 15 Jupiter-radii ($R_J \approx 71500$ km), the magnetic and plasma environment near the moon will be heavily impacted by the position of Ganymede relative to the plasmasheet (magnetodisc current sheet). Ganymede will be alternately located, in a periodic manner, between being immersed inside the Jovian plasmasheet, and just outside, in the so-called lobe regions. Ganymede's magnetosphere continually interacts with the corotating plasma in this plasma sheet. At this distance, the ambient plasma rotates somewhat more slowly than Jupiter itself. The local plasma rotation speed represents a subcorotation with respect to the planet, moving at 80% of the local corotation velocity (Kaweeyanun et al., 2020), which still greatly exceeds Ganymede's own orbital velocity.

The morphology of the magnetosphere of Ganymede is also quite different when compared to the magnetospheres of other planetary bodies in the Solar system, as due to the sub-Alfvénic and subsonic nature of the incident flow (Kaweeyanun et al. (2020); Khurana (1997)), there is no bow shock upstream of the moon and its magnetopause shape more closely resembles that of a pair of tilted cylinders, rather than the typical paraboloid or bullet-shaped form of other planetary magnetospheres. The tilt of these cylindrical features of Ganymede's magnetosphere arises because they are associated with two large Alfvénic wings that extend almost vertically along the moon's rotation axis (Jia & Kivelson, 2021) and where open field lines, formed through magnetic reconnection, link Ganymede to Jupiter's ionosphere. Near the moon's equator, the field structure mainly consists of closed magnetic field lines with both footpoints on Ganymede's surface. Close to the equator, these closed field lines are aligned roughly antiparallel with Jupiter's upstream magnetic field lines due to the 176° tilt of Ganymede's magnetic dipole with respect to its rotational axis (Kivelson et al., 2002), while open field lines, connecting to Jupiter, permeate the higher latitudes.

In these magnetically open regions, particles are able to escape Ganymede's magnetosphere into the surrounding Jovian environment, or precipitate from there towards Ganymede, giving rise to the formation of auroras around both the north and southern polar boundaries between the open- and closed-field-line regions (Saur et al., 2015). Importantly, there is also evidence for an induced magnetic field thought to be generated by the interaction of Jupiter's time-varying (rotating) magnetic field and conducting subsurface ocean layers in the interior of Ganymede, as discussed by Kivelson et al. (2002), located just a few kilometers below the surface of the moon. The possibility of a life-sustaining subsurface ocean constitutes a strong motivator towards developing a better understanding of this kind of moon-magnetosphere interaction and the interior structure of Ganymede itself. Magnetic field measurements taken during flybys of spacecraft are crucial for the characterisation of these putative subsurface layers, but the interpretation of such data requires a detailed understanding of each underlying contribution towards the total, observed magnetic field.

In this study we present an application of the UCL-AGA magnetodisc model (MDISC) developed by Achilleos et al. (2010), and updated by Millas et al. (2023), in order to study the magnetic and plasma conditions in the near-Ganymede space, as well as the periodically varying conditions upstream of Ganymede, which include the 'driving field' responsible for the induced response of the Ganymede ocean. We compare our model pre-

dictions with magnetometer measurements acquired by Juno on its most recent flyby of Ganymede and analyse how changes in the global plasma configuration and size of the Jovian magnetosphere can impact the overarching magnetic environment near Ganymede. Lastly, we compare our results with statistical fits of magnetic field data taken from multiple Galileo flybys in the vicinity of Ganymede's orbit - which may be taken to represent 'typical' field structure near Ganymede, at least during the Galileo mission epoch.

2 Magnetodisc Model Description

The UCL-AGA magnetodisc model is based on the original theoretical work of Caudal (1986), who developed a self-consistent model of Jupiter's magnetodisc field structure, derived from imposing a physical force balance between the centrifugal, magnetic and plasma pressure forces within the system. Caudal's proposed model is axisymmetric with respect to the planet's magnetic/spin axes, which in his picture are assumed to coincide (this makes the problem far more tractable for finding magnetic field solutions), and expresses the magnetic field as the result of the cross product between two Euler potentials, α and β_E:

$$\mathbf{B} = \nabla\alpha \times \nabla\beta_E \tag{1}$$

where the subscript E was introduced from the original Euler potential defined by Caudal (1986) as to avoid any confusion with the plasma β. The condition of $\nabla{\cdot}B = 0$ is also automatically satisfied by this definition of the field, as it results from the cross product of the two Euler potentials. Both of these quantities are general functions of the system's spherical coordinates r, φ, θ, which correspond to the radial distance from the planet's centre (in units of planetary radii), longitude and colatitude values, respectively, with respect to the planet's axis of rotation. As such, by exploiting the axisymmetry of the system, we are able to express these quantities as:

$$\begin{aligned} \alpha &= \alpha(r,\theta) \\ \beta_E &= R_p\varphi \end{aligned} \tag{2}$$

where R_p corresponds to the planet's radius. By considering only a meridional cut of the system, such that φ, and by consequence β_E, remain constant, we are able to omit β_E from the rest of this analysis. With this assumption, the magnetic field's radial component B_r and meridional component B_θ, are able to be solely expressed as a function of the derivatives of α:

$$\begin{aligned} B_r &= \frac{1}{r^2\sin\theta}\frac{\partial\alpha}{\partial\theta}, \\ B_\theta &= -\frac{1}{r\sin\theta}\frac{\partial\alpha}{\partial r} \end{aligned} \tag{3}$$

In order to achieve force balance for both the radial and meridional directions between the magnetic force (cross product of magnetic field and current density), pressure gradient and centrifugal forces in the rotating plasma one must satisfy the condition:

$$\boldsymbol{J}\times\boldsymbol{B} = \nabla\boldsymbol{P} - n\,m_\mathrm{i}\,\omega^2\,\rho\,\boldsymbol{e}_\rho \tag{4}$$

where $\boldsymbol{J}$ is the current density, $\boldsymbol{B}$ the magnetic field, $\boldsymbol{e}_\rho$ the outward unit vector in the direction perpendicular to the magnetic axis and $\rho = r\sin\theta$ the cylindrical radial distance from the planet. Caudal showed that the total plasma pressure, which is obtained from the cold and hot plasma populations, as well as the centrifugal force, can also be

expressed as functions of α, such that the force balance equation is able to be expressed by:

$$\frac{\partial^2 \alpha}{\partial r^2} + \frac{1-\mu^2}{r^2}\frac{\partial^2 \alpha}{\partial \mu^2} = -g(r,\mu,\alpha) \quad , \tag{5}$$

where $\mu = \cos\theta$ and g corresponds to the source function determined by the global distribution of plasma pressure and angular velocity, which can be used to derive the azimuthal current density J_ϕ:

$$J_\phi(r,\mu) = \frac{g(r,\mu)}{r\sin\theta} = \frac{g(r,\mu)}{\rho} \quad , \tag{6}$$

which constitutes a key element to the stretching of field lines near the magnetic equator.

The original method by Caudal then constrained the initial conditions of the physical parameters of the plasma along the equatorial plane, such as its density, temperature and flux tube content (number of ions in a tube with cross section of unit magnetic flux), by using the measurements taken by the Voyager 1 spacecraft. These observed equatorial properties act as boundary conditions for the global plasma properties within Caudal's formalism. A hot plasma population is then added to the system, with its content being modelled by the product of the equatorial hot plasma pressure, P_h, and the unit flux tube volume, V_h:

$$K_h = P_h V_h \tag{7}$$

with K_h being the hot plasma index, as introduced by Achilleos et al. (2010) and Millas et al. (2023), which is assumed to decline linearly with decreasing distance inside ~ 10 Jupiter radii (R_J) and remain constant for radial distances outside this range.

The initial conditions for the equatorial angular velocity as a function of the equatorial distance ρ used by Caudal is obtained from Hill's theory (Hill, 1979), and derives from the conservation of plasma angular momentum and magnetic flux for the case of a simple magnetic dipole field. The final step in Caudal's model is then to apply an iterative process to numerically solve the force balance equation (**Equation 5**) by expanding the function α in terms of Jacobi Polynomials, in order to satisfy the homogeneous part of the differential equation, obtaining the following solution:

$$\alpha_{\mathrm{H}}(r,\mu) = \left(1-\mu^2\right)\sum_{n=0}^{\infty} C_n r^{-(n+1)} P_n^{1,1}(\mu) \tag{8}$$

as demonstrated by Achilleos et al. (2010). The homogeneous solution is then restricted to just its first order term, corresponding to the magnetic potential associated with the internal dipole field of the planet:

$$\alpha_{dip} = \frac{1-\mu^2}{r} \tag{9}$$

Furthermore, the plasma source function g is given by the expression:

$$g(r,\mu,\alpha) = \rho^2 \frac{\mathrm{d}P_{\mathrm{h0}}}{\mathrm{d}\alpha} + \rho^2 \exp\left(\frac{\rho^2-\rho_0^2}{2\ell^2}\right)\frac{P_{\mathrm{c0}}}{\ell^2 B_{\theta 0}} \tag{10}$$

with P_h and P_c denoting the hot and cold plasma pressures, with the subscript 0 used to refer to quantities evaluated at the equatorial crossing point of the corresponding magnetic field line. The equatorial pressure and angular velocity profiles are provided through spacecraft in situ measurements.

Within this theoretical framework, it is then possible to obtain the full, albeit cumbersome, solution for α as a function of g, by adding the homogeneous solution with the non-homogeneous solution, as follows:

$$\begin{aligned}\alpha(r,\mu) = &\frac{1-\mu^2}{r} \\ &+ \left(1-\mu^2\right)\sum_{n=0}^{\infty}\frac{P_n^{1,1}(\mu)}{2n+3}\left[r^{n+2}\int_r^{\infty} g_n(u)u^{-(n+1)}\mathrm{d}u\right. \\ &+ r^{-(n+1)}\left(\int_{r_c}^{r} u^{n+2}g_n(u)\mathrm{d}u\right. \\ &\left.\left.-r_c^{2n+3}\int_{r_c}^{\infty} u^{-(n+1)}g_n(u)\mathrm{d}u\right)\right]\end{aligned} \tag{11}$$

with u being a dummy-variable of the radial distance r in normalised units of Jupiter radii and g_n corresponding to the expansion coefficients of the source function g. We refer the reader to the paper by Achilleos et al. (2010) for a detailed demonstration of such a solution. As an initial condition, the magnetic field is assumed to be a dipole, such that:

$$\alpha_0 \equiv \alpha_{dip} = \frac{1-\mu^2}{r}. \tag{12}$$

Combining this initial form, or 'estimate', for the solution α with **Equation 10**, we are able to then determine the global values for the source function g across the model domain and, then, use them in conjunction with **Equation 11** in order to obtain an 'intermediate' value of the magnetic potential, α'. From this, we are then able to define, for reasons of numerical stability, the next iteration of the function α as a linear combination of the 'old' iteration and the 'intermediate' solution derived from that iteration, as given by:

$$\alpha = \nu_{i-1}\alpha_{i-1} + \nu_i\alpha_i' \tag{13}$$

where ν_{i-1}, ν_i are the fractions of the 'old' iteration and 'intermediate' solution, respectively, with α now representing the next iteration to be used in the next cycle of source function and updated solution calculation. In principle, any combination of ν_{i-1} and ν_i, each bound to the interval $[0, 1]$, could be used, as long as they satisfy the condition of $\nu_{i-1} + \nu_i = 1$. In his study, Caudal used equal fractions for the two solutions ($\nu_{i-1} = \nu_i = 0.5$). By introducing this 'mixing' of solutions we are able to stabilise the convergence towards a final solution of α. The iterative process would continue until a certain threshold condition for the difference between iterations is achieved. This way, we are able to obtain a more complex description of the magnetic field observed in the Jovian system, which presents a dipole-like behaviour close to the planet and smooth transition to the magnetodisc structure at larger equatorial distances.

The UCL magnetodisc model, introduced by Achilleos et al. (2010), consists of a numerical implementation of Caudal's model. In their study, an adaptation of Caudal's original methods for the modelling of Jupiter's magnetosphere is presented in order to apply them to the Saturnian case. Millas et al. (2023) also provided further improvements to the 'Jovian mode' of this model, such as adjustments to the equatorial plasma conditions and hot plasma pressure, with the introduction of newer datasets obtained through

measurements taken by the Galileo spacecraft (as also explored by Nichols et al. (2015)), and updates to the plasma's angular velocity profile using Pontius' method (Pontius, 1997), as to acquire a plasma ω fully self-consistent with the magnetic field.

The need for a new approach to the determination of the angular velocity profile arises as a byproduct of Caudal's adjusted magnetic field morphology, as the original profile given by Hill (1979) is only applicable to the magnetic dipole scenario. As such, Millas et al. (2023) implemented Pontius' correction to this problem, which uses information from the more complex magnetic field structure obtained from Caudal's model, defined by the so called Pontius equation (Pontius, 1997) expressed by:

$$L^5 \frac{df}{dL} + \left[2L^4 + 4L_o^4 \mu_B \cos\left(\theta(r)\right)\right] f - 2L^4 = 0 \tag{14}$$

with L corresponding to equatorial crossing distance (in units of planet radii) of a field line; and $f = 1 - \omega/\omega_J$ to the corotation lag between the angular velocity of the plasma, ω, and the angular velocity of Jovian planetary rotation, ω_J. The $\cos\left(\theta(r)\right)$ term, the so called 'mapping function', connects a given point along the magnetic equator, at radial distance r, to a footpoint of colatitude θ in Jupiter's ionosphere, by following a magnetic field line of constant α. The scaling dimensionless term L_0 is defined as:

$$L_o^4 = \pi \Sigma_p R_p^2 B_p^2 / \dot{M} \tag{15}$$

and is a function of the planetary radius R_p, the equatorial magnetic field B_p, the height-integrated Pedersen's conductivity Σ_p and the total plasma outward mass flow rate $\dot{M}$. Lastly, μ_B corresponds to the 'Pontius number', which encodes the difference between the more realistic description of the magnetic field structure obtained from Caudal's method and the simple dipole model, and is expressed as:

$$\mu_B = \frac{B_r^i(\theta)}{B_{r,dip}^i} \cdot \frac{B_z^{eq}(\rho)}{B_{z,dip}^{eq}} \rho \sin^2\theta \tag{16}$$

with the fractions $B_r^i(\theta)/B_{r,dip}^i$ and $B_z^{eq}(\theta)/B_{z,dip}^{eq}$ being associated, respectively, with the deviations in ionospheric radial field and equatorial axial field components, compared to the dipole model.

For short radial distances, or when far from the magnetic equator, the dipole field gives a good approximation to the observed magnetic structure, and so, under such conditions, $\mu_B \sim 1$ and we are able to use Hill's angular velocity profile. In it, ω is considered to be uniform all the way along a magnetic field line from disc to planet, for a steady state configuration of an equatorial disc of plasma (Ferraro, 1937). However, in order to determine the angular velocity profile for the magnetic structure given by Caudal's method, we must first express the mapping function for this more complex scenario. This can be done by taking advantage of the constant α values along a given field line and using the magnetodisc model results in order to numerically determine $\cos\left(\theta(r)\right)$. We are then able to use **Equation 14** in order to determine a new angular velocity profile, which could then be used in order to further adjust the value of α as an additional component of a similar iterative process as the one described by Caudal for evaluating the source function g. We refer the reader to the study of Millas et al. (2023) where a full description of this new iterative process is given, as well as its relation to Caudal's original method.

In this work we present the application of the latest UCL magnetodisc model and compare its predictions with the magnetic field measurements taken by Juno during its latest flyby of Ganymede. To do so, we make use of reference frame transformations to

project the spacecraft's position from the rotating jovigraphic reference frame, typically used in Juno data releases, to the jovimagnetic reference frame, whose z-axis is aligned with the planet's magnetic axis, which possesses a tilt of $\theta_d = 10.31°$ with respect to its rotational axis, and the x-axis along the magnetic equator and pointing towards jovigraphic longitude $\phi_d = 163.39°$ (Connerney et al., 2018). The magnetic field measurements taken by Juno are also converted into this new reference frame in order to be correctly compared with the model's output. Using this approach, we are then able to take full advantage of the model in order to also predict the plasma environment the spacecraft encountered at any given point along its trajectory through the Jovian system. Moreover, we are able to use the field and plasma properties of our best-fitting model in order to make predictions regarding the expected periodic variations in magnetic field, plasma pressure, and dynamic pressure of plasma rotation, upstream of Ganymede itself. This represents a prediction analogous to that presented by Achilleos et al. (2014) who used the model in 'Saturn' model to predict magnetic and plasma pressures in the rotating magnetospheric plasma upstream of Saturn's moon, Titan.

3 The PJ34 Trajectory and MAG Dataset

The MAG PJ34 dataset comprises positional and magnetic field data taken during the 34th perijove pass of the Juno spacecraft, which spanned from 13th May until 29th June, 2021. This particular trajectory included a flyby of Ganymede, reaching a periapsis altitude of just 1000 km above the moon's surface, on 7th June, 2021. In **Figure 1**, we show a portion of the PJ34 trajectory (13:34:31 UT, 6th June to 02:31:31 UT, 10th June, 2021) as depicted in the jovimagnetic reference frame, superposed with a colourmap of the logarithm of the hot plasma pressure predicted by the MDISC model (for input parameters $K_h = 2.719 \times 10^7\,\mathrm{Pa\,m\,T^{-1}}$ and $r_{\mathrm{max}} = 79.5\,R_J$).

During its inbound pass, the spacecraft travels near the magnetic equatorial plane, crossing the current sheet multiple times on its way towards Jupiter. The encounter with Ganymede is made at approximately $15\,R_J$, reaching its periapsis at 16:56:08 UT on 7th June, 2021. The spacecraft then continues its approach of Jupiter, completing its 34th perijove less than one day later (07:45:49 UT, 8th June, 2021), before heading towards the planet's outer magnetosphere once again. This time, the flight-path oscillates around the model's last closed field line, far from the equatorial plane.

In this study we will analyse the magnetic field measurements taken by Juno's MAG instrument suite, which consists of two boom mounted observing platforms, each equipped with a vector fluxgate magnetometer (FGM) among other instruments. Each of these FGMs are capable of measuring the magnetic field in three components of the vector field, with only one of these devices being powered at any given time and placed two meters apart from one another, in order to provide redundancy and allow the capability to monitor spacecraft-generated magnetic fields during the flight. The performance characteristics of the instrument can be found in the paper by Connerney et al. (2017). All the magnetic field results presented in this paper fall well within Range 0 of the instrument, meaning that the expected error associated with these measurements is expected to be $< 0.1\,\mathrm{nT}$, or a relative error of order $\sim 0.1\%$ for typical field strength near Ganymede.

In the next sections, we present a detailed analysis of the magnetic field measurements taken during the PJ34 trajectory, how they compare with the results predicted by the UCL magnetodisc model and with previous similar studies of Galileo data taken in the vicinity of Ganymede's orbit. We also analyse the plasma environment using the magnetodisc model and make predictions regarding the periodic behaviour of the different pressure components along the PJ34 trajectory and the orbit of Ganymede. These specifically include plasma pressure from the cold and hot particle populations, dynamic pressure associated with bulk rotation of plasma, and magnetic pressure.

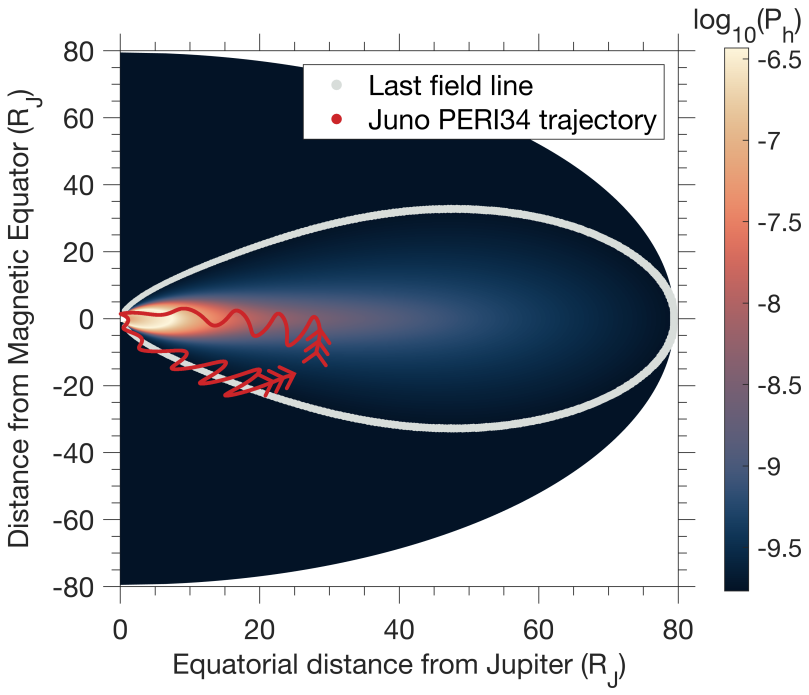

Figure 1. Juno PJ34 trajectory (red) in the jovimagnetic reference frame plotted over a logarithmic colour map of the hot plasma pressure (P_h) normalised through division by B_o^2/μ_0, where $B_o = 428\,000\,\mathrm{nT}$ is the approximate equatorial field strength at the surface of Jupiter. The two arrows show the spacecraft's direction of motion along the inbound and outbound phases of the trajectory. The predicted hot plasma pressure values were obtained using values of $K_h = 2.719 \times 10^7\,\mathrm{Pa\,m\,T^{-1}}$ and $r_{\max} = 79.5\,R_J$.

4 Comparison of Magnetodisc Model and Juno PJ34 Observations

In **Figure 2** we show the total magnetic field predicted by the MDISC model along the PJ34 trajectory, as well as a colourmap of the ratio of the current sheet field strength compared to that of the Jovian dipole (internal) field, with both quantities also being provided by the MDISC model, at each position of the spacecraft's trajectory. The positional data used here, and for which we are predicting the magnetic field using our model, results from a 60-second downsampling of the original, higher frequency, magnetic and positional data taken by the spacecraft in order to diminish small-scale fluctuations. An inner cutoff point of $9.6\,R_J$ was imposed because, at that equatorial distance from the planet, the magnitude of the field due to magnetodisc currents corresponds to $\sim 20\,\%$ of the dipole field magnitude. The outer cutoff point was fixed at $30\,R_J$ as it corresponds to roughly twice the orbital radius of Ganymede, thus providing good coverage of the middle magnetosphere near Ganymede orbit. Over the course of this paper, we will focus our analysis on this portion of the trajectory and shall refer to it as simply the PJ34 trajectory, since we are mostly interested in analysing the ambient magnetic and plasma environment in the near-Ganymede space.

Current sheet crossings are marked by local minima in the magnitude of the magnetic field, corresponding to points where the spacecraft traverses the magnetic hemispheres. In contrast, the exterior or lobe regions of the current sheet, corresponding to locations further away from the magnetic equator, are associated with broader local maxima in magnetic field strength. In the following sections, we will analyse in further de-

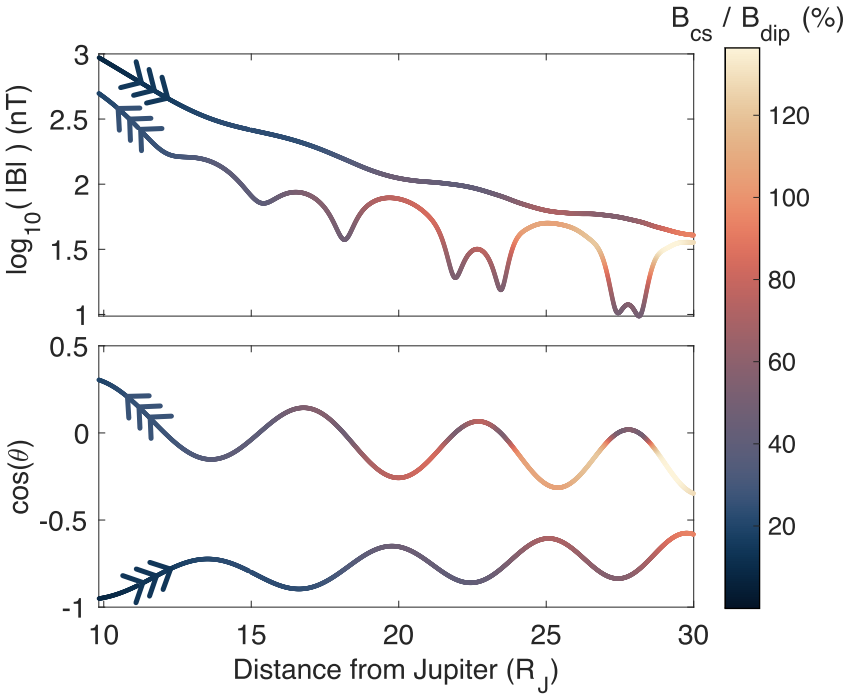

Figure 2. Logarithm of the magnetic field magnitude and cosine of colatitude (θ) versus radial distance in Jovian radii during a portion of the PJ34 trajectory, plotted with a colourmap of the percentual relative strength of the current sheet field compared to the planetary dipole. Both the inbound and outbound portions of the PJ34 trajectory are shown, with the spacecraft's direction of motion during each depicted by the arrows. The inner cutoff point was defined as the distance for which the magnetodisc currents' field strength becomes 20 % of the dipole field's, whereas the outer cutoff point was fixed at 30 R_J, corresponding to roughly twice the orbital radius of Ganymede.

tail the cylindrical components and magnitude of the magnetic field over the course of the PJ34 trajectory.

The relative strength of the current sheet field can be seen varying both with the spacecraft's distance from Jupiter and with its altitude above or below the magnetic equator. During the inbound pass of the trajectory, the current sheet field achieves a maximum relative contribution for the exterior regions of the current sheet, achieving a higher intensity than the Jovian dipole field for distances greater than $\sim 25\,R_J$. However, this contribution is seen to decrease over time, as the spacecraft's flight-path not only brings it ever closer to the planet, but also gradually reduces its mean altitude with respect to the magnetic equator. Nonetheless, the current sheet field can be seen to provide a very significant contribution during the majority of the inbound pass. As for the outbound pass, the magnetodisc current field progressively increases in relative importance as the spacecraft heads towards the middle magnetosphere, achieving the same intensity as Jupiter's dipole field at $\sim 30\,R_J$, a higher radial distance than the one recorded for the inbound phase, due to Juno now travelling far below the magnetic equator. The field structure observed during this stage of the trajectory is largely dictated by the Jovian dipole field with significant contributions from the magnetodisc current, depending on altitude and distance.

4.1 Analysing the Magnetic Field Components

In order to analyse how well the MDISC model is able to predict the behaviour observed by Juno, we must first determine both the **hot plasma index** (K_h), as defined by **Equation 7**, and **effective magnetodisc radius** ($r_{\max}$) during the encounter, which approximately translates to the local time sector distance to the magnetopause (Sorba et al., 2019). This was done by fitting the magnetic field components B_ρ and B_z, in cylindrical coordinates, and analysing the performance of the model via a chi-square goodness of fit test for a wide range of magnetospheric parameters. Due to the poloidal nature of the field and the absence of radial currents in the magnetodisc model used, no azimuthal component B_ϕ can be obtained, hence this component was not included in the parameter fitting. We provide further detail of the fitting process in **Appendix A**, as well as an analysis of the model parameters and their associated uncertainties. Our best fit, based on minimisation of the difference between model and data field components, was achieved with the nominal values of $K_h = 2.719{\times}10^7\,\mathrm{Pa\,m\,T^{-1}}$ and $r_{\max} = 79.5\,R_J$ for the two fitted parameters, respectively.

In **Figure 3**, we present the magnetic field measurements taken by Juno during its PJ34 trajectory, as well as the ones predicted by the magnetodisc model using this optimal set of fitted magnetospheric parameters, further detail being presented in **Table A1**. We also show a comparison between the azimuthal component of the magnetic field, B_ϕ, measured by Juno with ΔB_ρ, the radial field due to the current sheet only, which is defined by the results of subtraction between the radial component of the observed magnetic field and the radial component coming from a model of Jupiter's internal dipole with an equatorial field strength of $\sim 428\,000\,\mathrm{nT}$ (Smith et al., 1975). For this analysis, we utilise the same radial distance restrictions illustrated in **Figure 2**.

The model results are in good agreement with the in situ measurements taken by the spacecraft for the majority of the trajectory, with both the amplitude and phase of the periodic oscillations in the magnetic field being well captured by the model, resulting in a combined root-mean square error value of $\sigma = 7.72\,\mathrm{nT}$ calculated using the radial, B_ρ, and the axial component, B_z, of the magnetic field.

Regions of significant variability in the measurements can be observed during current sheet crossings, where there exists a higher relative density of plasma, with the intensity of these fluctuations increasing with radial distance from the planet. It is especially in these regions where we can see a clear anti-phase relation between Juno's az-

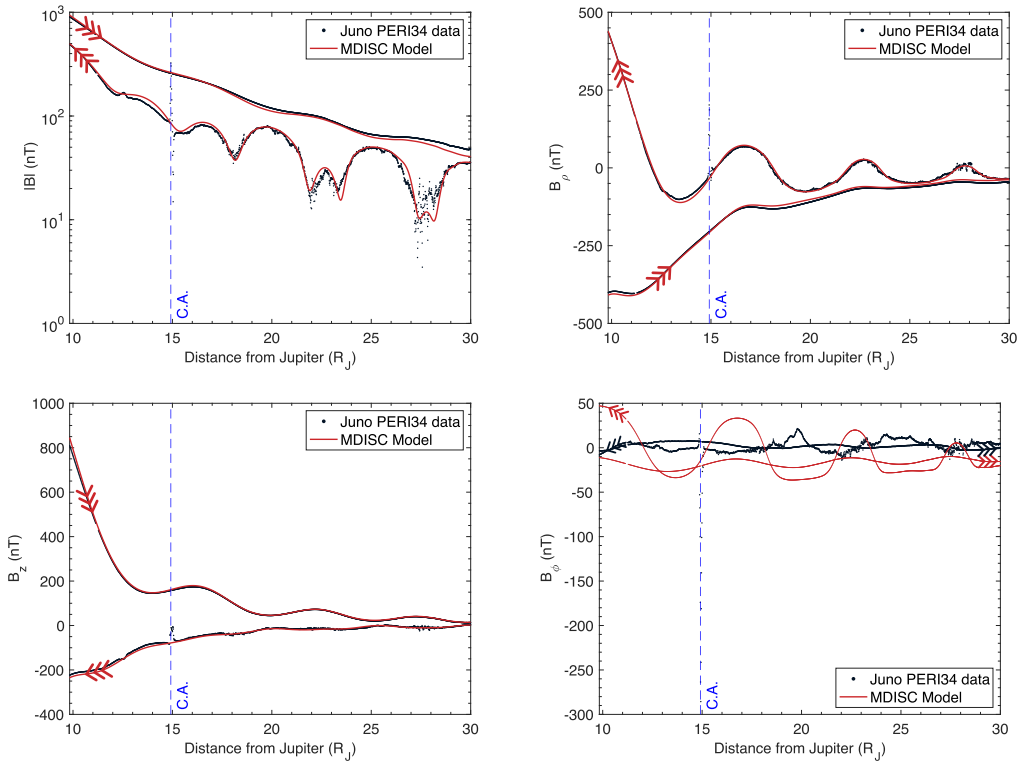

Figure 3. Jovimagnetic cylindrical components and magnitude of the magnetic field measured by Juno (black) and predicted by the magnetodisc model (red), as a function of distance from Jupiter, during the PJ34 trajectory. A comparison between the measured B_ϕ component and ΔB_ρ resulting from the magnetodisc model is also shown (bottom-right). The Ganymede encounter's closest approach point is marked on each of plots, 'C.A.', and only occurs during the inbound phase of the trajectory. The model results are in good agreement with the in situ data obtained by the spacecraft on both the components and magnitude of the magnetic field taken over the entire trajectory shown, with the exception of the Ganymede encounter, since the model does not inherently possess any contributions coming from the moon's internal field, nor its own magnetospheric environment. The signature of Jupiter's oscillating magnetodisc can be observed from, for example, the anti-phase relation between B_ϕ and ΔB_ρ, as opposed to the quarter-cycle phase relation expected from a pure dipole field (Khurana & Kivelson, 1993).

imuthal component of the magnetic field and the ΔB_ρ given by the model, which corresponds to the typical phase relations of a magnetodisc current sheet field. Contrarily, for a pure dipole field one would expect to observe a quarter cycle phase mismatch (see Khurana and Kivelson (1993)). This signature is also best observed during the inbound phase of the trajectory, as its flight-path takes the spacecraft closer to the magnetic equator, thus resulting in a stronger field contribution coming from the current sheet field, as shown in **Figure 2**. For the outbound phase of the trajectory, this relation between the two quantities becomes much harder to discern, due to the much lower amplitudes of the oscillating field components, a result of the spacecraft remaining far below the magnetic equator. During the later portion of the PJ34 trajectory, an increasingly poorer agreement between the model predictions and the measurements can be observed, suggesting a possible variation in the magnetospheric configuration over time. Although in this work we focus on the determination and analysis of the behaviour resulting from a

set of fixed, best-fitting parameters to the entirety of the PJ34 trajectory, one could, in principle, use a 'rolling window' approach to study the time evolution of the Jovian magnetospheric configuration using this type of model. Bunce et al. (2007) provides a similar approach to this, where the best fitting magnetospheric parameters of their ring current model of Saturn are determined in order to estimate the magnetopause distance over the course of several Cassini orbits. We leave such an exercise for a future study.

The Ganymede encounter, which occurred during the orbit under consideration, can be identified by the clear signature observed in all components of the magnetic field at around 15 R_J. This abrupt change in the ambient magnetic field is largely due to the significant contribution of Ganymede's own internal magnetic field, which increases as the spacecraft approaches the moon, as made evident in the zoomed plots shown in **Figure 4**. For these, a higher-frequency average sampling of 1 second was used, instead of the 60-second average used for the previous analysis of the entire PJ34 trajectory.

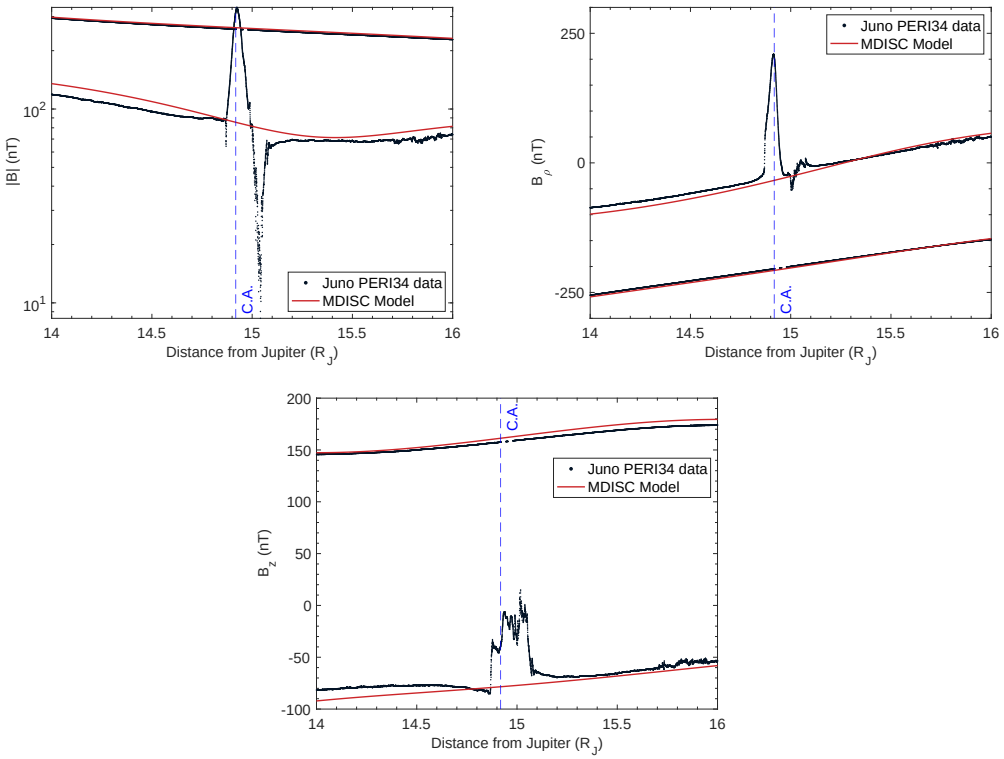

Figure 4. Close up view of the jovimagnetic magnitude and cylindrical components of the magnetic field measured by Juno (black) and predicted by the magnetodisc model (red), as a function of distance from Jupiter, during the Ganymede encounter portion of the PJ34 trajectory. We also show the same distance interval from the other pass of this orbit (not containing Ganymede encounter), for comparison purposes.

Since the magnetodisc model does not include any magnetic field contribution coming from Ganymede nor its magnetosphere, the model, of course, fails to reproduce the observed magnetic environment during the flyby and the transition regions between Jupiter's ambient and Ganymede's smaller magnetosphere. However, we can see that Ganymede's influence is rather spatially limited as, just a few Jupiter radii away from the moon, the Jovian ambient field once again becomes the dominant field contribution, with better agreement once again attained with model prediction. This result suggests, however, that

it would be possible to use the model's outputs, in a modified form, to estimate ambient field and plasma variability upstream of Ganymede at the time of closest approach. Similar predictive use of the UCL MDISC model, in its 'Saturn' mode, was explored by Achilleos et al. (2014), who were considering the Titan-Saturn interaction.

4.2 Influence of Ganymede's Intrinsic Field

As observed, Ganymede's internal magnetic field assumes a vital role in dictating the magnetic environment close to the moon. In order to attempt to determine how the interaction between this field and the ambient Jovian field gives rise to the complex field rotations shown in **Figure 4**, we add to the existing magnetodisc model an additional, simple dipole field, centred on Ganymede, with an equatorial field strength of 719 nT. For simplicity, we aligned its magnetic moment along Jupiter's spin axis, but pointing southward, so as to approximate Ganymede's 176° magnetic moment tilt (Kivelson et al., 2002) and low inclination of its orbital plane of 0.20° with respect to Jupiter's equator (Jacobson, 2014). In **Figure 5** we show the predicted field components from the combined magnetodisc-plus-simple-dipole model.

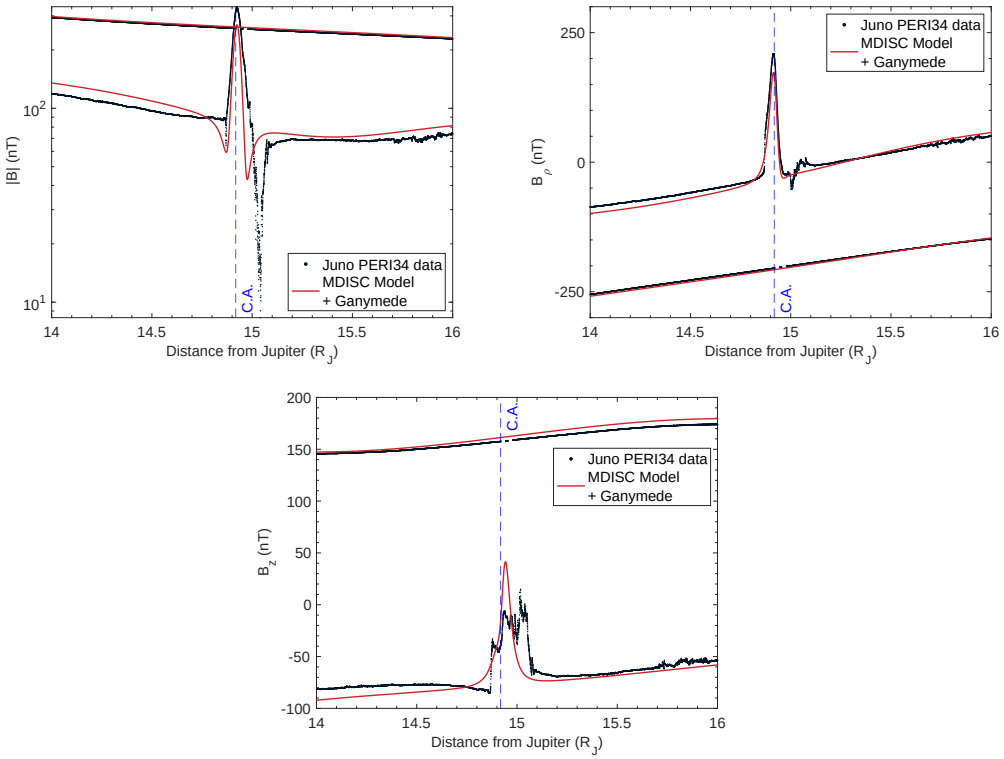

Figure 5. Close up view of the comparison between the jovimagnetic magnitude and cylindrical components of the magnetic field measurements (black) and predicted values by the magnetodisc model (red), with the addition a simple dipole field for Ganymede's intrinsic field, during the Ganymede encounter. In each plot, the line with the clear signature of the encounter corresponds to the inbound phase, while the other corresponds to the outbound phase of the trajectory. We do not expect this first approach to fully capture the higher order variability in the magnetic field components and magnitude, but it achieves fairly good agreement for the radial component.

Our simple first approach is not a complete model, since there is a far more complex connection between the two magnetospheres, including field due to current sheets on Ganymede's magnetopause and in the interior of its magnetosphere (Stone and Armstrong (2001); Jia et al. (2008)). Even so, we find reasonable agreement for the general trends exhibited by the radial component of the field vector, thus suggesting that additional field contributions would mainly affect the other field components during this flyby. Indeed, we observe in the figure that B_z would seem to be much more affected by other field sources, giving rise to higher order fluctuations, beyond the capability of the model to reproduce.

Now considering the magnitude of the magnetic field, we observe a contrasting scenario, where, during the inbound phase of the Ganymede encounter, the model fails to reproduce the observed behaviour, as opposed to the outbound phase where it achieves fairly good agreement with the measurements taken by Juno. A more detailed modelling of the intrinsic and induced field contributions, as well as the transition region between the two magnetospheres, would be needed in order to model the higher order variations observed during the encounter. Nonetheless, these results show promise to a future vacuum superposition approach, consisting of combining the UCL-AGA magnetodisc model with other Ganymede environmental magnetic field models, in order to achieve a better characterisation of the full magnetic environment that surrounds the Jovian moon.

4.3 Impact of Magnetospheric Size and Hot Plasma Content on Field Structure

In this section, we analyse how variations in the fitted magnetospheric parameters may improve the agreement between the predictions given by the MDISC-plus-Ganymede-dipole approach and the magnetic field measurements taken by Juno during its encounter with Ganymede. Utilising the same framework as the one used by Romanelli et al. (2022), we analyse the impact of such changes in the different components and magnitude of the magnetic field, using the Ganymede centred Phi-Omega (GPhiO) reference frame with the following axis orientations: X pointing along the incident Jovian plasma flow direction, Y directed along Ganymede-Jupiter vector (positive toward Jupiter), and Z being parallel to Jupiter's spin axis. In **Figure 6**, we show the results of this comparison for the optimal set of parameters, as well for both a compressed and expanded Jovian magnetosphere. For the compressed version, values of $K_h = 1 \times 10^7\,\mathrm{Pa\,m\,T^{-1}}$ and $r_{\max} = 60\,R_J$ were used, whereas values of $K_h = 3 \times 10^7\,\mathrm{Pa\,m\,T^{-1}}$ and $r_{\max} = 90\,R_J$ were used for the expanded case, such that any other reasonable set of magnetospheric parameters will result in an intermediate behaviour between these 'bounding scenarios'. Once again, due to the focus on the small time-frame of the Ganymede flyby as used by Romanelli et al. (2022), an average data sampling of 1 second was used for this analysis.

The results show modest agreement, at times, between the different field components and magnitude of the magnetic field predicted by the model and Juno's measurements. Once again, higher order fluctuations can be seen on all panels, particularly during the inbound phase of the encounter, pointing to a complex transition region between the two magnetospheres. For B_x, the field component pointing along the incident Jovian flow direction, the model fails to reproduce the total field intensity, despite managing to capture most of the overarching rotation of the observed field. Additional field contributions, particularly oriented opposing the incoming Jovian flow, appear to be needed in order to provide a better agreement with these measurements. The introduction of an induced magnetic field as described by Zimmer et al. (2000) could provide this necessary contribution, as the induced dipole generated by the time varying Jovian field would mostly be oriented such that the generated magnetic field would oppose the incoming Jovian field. Magnetic field contributions resulting from current sheets on Ganymede's magnetopause and in the interior of its magnetosphere can also provide a significant con-

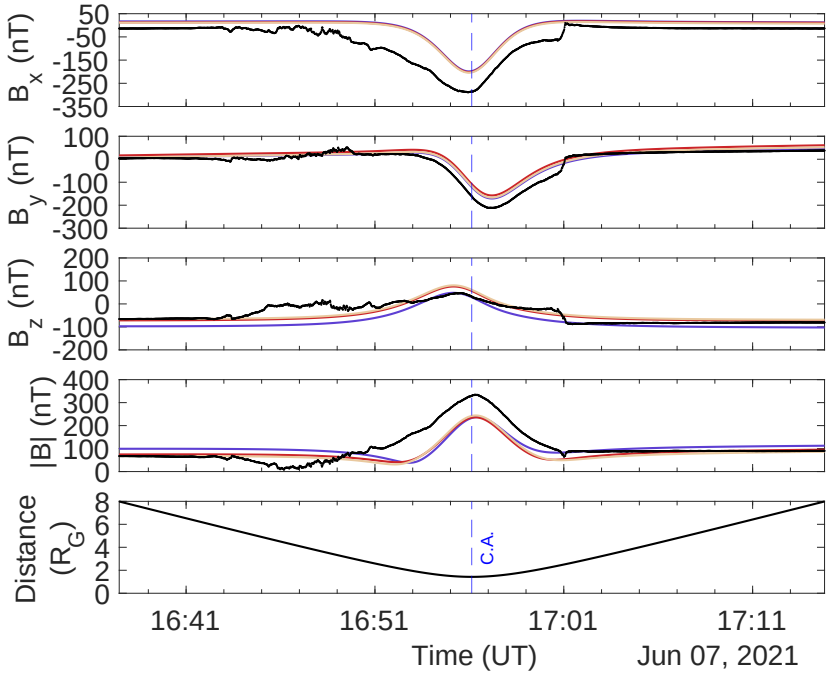

Figure 6. Magnetic field components of Juno's 1-second averaged MAG data (black) and predictions of the MDISC + Ganymede dipole model, as a function of time. The results show the model predictions for the optimal magnetospheric configuration (red), as well as a compressed (purple) and expanded Jovian magnetosphere (yellow). See text for the values of the associated parameters used. The distance to Ganymede during the encounter is also shown (bottom panel).

tribution to these field components, as discussed by Jia et al. (2008), where they were shown to enhance the B_z component and decrease B_x during several flybys of the Galileo spacecraft.

The field component B_y, which is oriented along the Ganymede-Jupiter direction, provides the best agreement with the Juno data, indicating that the magnetic field along this direction is mostly well-described by the combination of Ganymede's intrinsic magnetic field and the Jovian ambient field. In the case of B_z, the component oriented along Jupiter's spin axis or normal to the moon's orbital plane, we observe worse agreement during the transition region between the two magnetospheres as described in Romanelli et al. (2022), pointing once again towards the need of a more complex approach to model the behaviour observed in this region. However, once the spacecraft enters Ganymede's magnetosphere, the agreement shows some improvement, as Ganymede's magnetic field contributions increasingly approach the behaviour given by a dipole field, before worsening once again as the spacecraft moves away from the moon.

These results are in good agreement with the ones obtained by Romanelli et al. (2022), which used a global three-dimensional hybrid model that allows one to investigate plasma processes occurring in the magnetosphere of Ganymede (LatHyS), showing the attainability of such results using a more complete description of the plasma environment. Changes in the model's magnetospheric parameters can also provide further, although seemingly modest, improvements in the predicted behaviour, as shown in these results for the optimal, compressed and expanded configurations. These changes are particularly noticeable along B_z and in the magnitude of the magnetic field, with the former showing a vari-

ation of $\sim$ 33 nT across the entire encounter, and the latter showing variations up to that same value when relatively far from the moon, as shown in **Figure 6**. The other field components, B_x and B_y, show negligible changes resulting from different magnetospheric parameters, presenting variations in the order of just a few nanotesla.

Overall, this analysis builds upon that of Romanelli et al. (2022) by providing estimates of how the magnetodisc field near Ganymede would respond to global reconfigurations of the magnetosphere, showcasing that the ambient field measurements upstream of Ganymede taken during flyby encounters, such as the case of the one during PJ34, provide a potentially important diagnostic of this global magnetospheric state, as summarised by the parameters representing system size and global energetic particle content.

5 Plasma Conditions During PJ34

In **Figure 7**, we present the magnetic and plasma pressures predicted by the magnetodisc model, without the addition of the Ganymede dipole, over the course of the PJ34 trajectory. These pressures are normalised by a factor of $B_0^2/\mu_0 = 0.146$ Pa, as described in Achilleos et al. (2010), with $B_0 = 428\,000$ nT being the mean intensity of the Jovian magnetic field at the planet's equator. Once again, these results were obtained using the optimal magnetospheric parameters (**Table A1**).

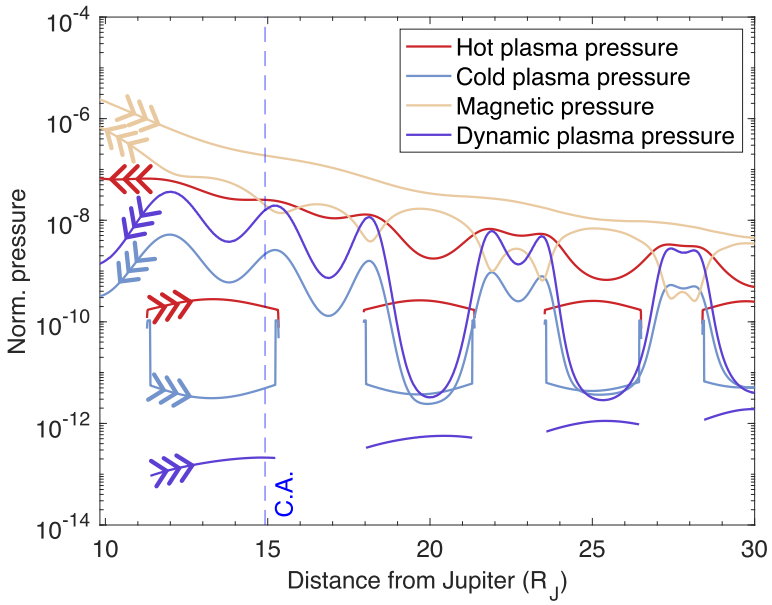

Figure 7. Predictions for the normalised hot (red), cold (blue), dynamic (purple) plasma pressures and magnetic pressure (yellow) given by the MDISC model, over the course of the PJ34 trajectory.

The hot plasma pressure provides the maximum pressure during current sheet crossings for the large majority of the trajectory, with the magnetic pressure assuming the dominant role when closer than $\sim 12\,R_J$. As for the regions outside the current sheet, the magnetic pressure constitutes the main contributor towards the total pressure of the system for the entirety of the trajectory. The hot, cold and dynamic plasma pressures show an anti-phase relation with the magnetic pressure, assuming maximum values dur-

ing current sheet crossings. For regions in between 12 and 25 R_J, both the hot and dynamic plasma pressures manage to surpass the magnetic pressure during these crossing events, with the cold plasma pressure achieving the same feat for distances greater than $\sim 24\,R_J$.

During the inbound phase of the trajectory, all pressures gradually increase over time, as the spacecraft comes ever closer to Jupiter. Contrarily, the difference in intensities between the plasma and magnetic pressures is seen to decrease over successive current sheet crossing events. As for the exterior regions of the sheet, both the dynamic and cold plasma pressures show a drastic decrease in intensity when compared with their values during crossings. The hot plasma pressure varies in a similar manner between plasma sheet interior and exterior, but with a much smaller change in amplitude. However, for radial distances between 20 and 17 R_J, this relative decrease in pressure intensities over the external regions of the current sheet becomes much less pronounced. This seemingly sudden change comes from a combination of two different factors. The first constitutes a progressive decrease in the relative impact of the magnetodisc in the plasma environment, particularly over the exterior regions, as the spacecraft approaches Jupiter. The associated reduction in field line extension greatly diminishes the plasma pressure's dependence with position relative to the current sheet. The second factor relates to a gradual change in the spacecraft's oscillating trajectory, as perceived in the jovimagnetic reference frame, which brings its mean position closer to the magnetic equator, as shown in **Figure 2**, thus giving rise to an overall increase in pressure and a more uniform plasma behaviour than the one marked by the interactions with the current sheet.

Considering the outbound portion of the PJ34 trajectory, the plasma environment is overwhelmingly dominated by the magnetic pressure, with periodic contributions coming from the plasma, as the spacecraft weaves in and out of the model's closed field line region of the Jovian magnetosphere, thus showing a much more stable and constant pressure value during this portion of the trajectory. Our results thus suggest that future plasma moments acquired from plasma data in this region of the magnetosphere would constitute an important diagnostic of the presence, or absence, of a natural plasma boundary of this kind.

6 Plasma Conditions Near Ganymede's Orbit

In **Figure 8**, we show the normalised hot, cold and dynamic plasma pressures, as well as the magnetic and total pressure, predicted by the magnetodisc model along Ganymede's orbit over the course of one Jovian synodic period. We also analysed the impact of the magnetospheric parameters in the predicted behaviour of the different pressures, showing results for a compressed magnetosphere, with $K_h = 1 \times 10^7\,\mathrm{Pa\,m\,T^{-1}}$ and $r_{\max} = 60\,R_J$, an expanded magnetosphere, with $K_h = 3 \times 10^7\,\mathrm{Pa\,m\,T^{-1}}$ and $r_{\max} = 90\,R_J$, and the optimal PJ34 configuration of $K_h = 2.719{\times}10^7\,\mathrm{Pa\,m\,T^{-1}}$ and $r_{\max} = 79.5\,R_J$.

As observed previously in our analysis of the plasma pressures during the PJ34 trajectory, the hot, cold and dynamic plasma pressure assume an anti-phase relation with the magnetic pressure, having maximum values during current sheet crossings. The hot and dynamic plasma pressures manage to overpower the magnetic pressure during these crossings, while the latter assumes a dominant role in the exterior regions of the current sheet, as seen in **Figure 7**, given that Ganymede orbits Jupiter at around $\sim 15\,R_J$. The cold plasma pressure assumes a lesser role, being by far the weakest contributor to the overall pressure of the system in the vicinity of Ganymede's orbit. When compared to the case of Titan and the Saturnian system as presented by Achilleos et al. (2014), a similar picture is presented, where the relative importance and fluctuation intensity of the plasma pressures is somewhat similar between the two cases. However, they also show some notable differences, where in this case the cold plasma pressure never surpasses the magnetic pressure, something that *does* occur during current sheet crossings near Titan.

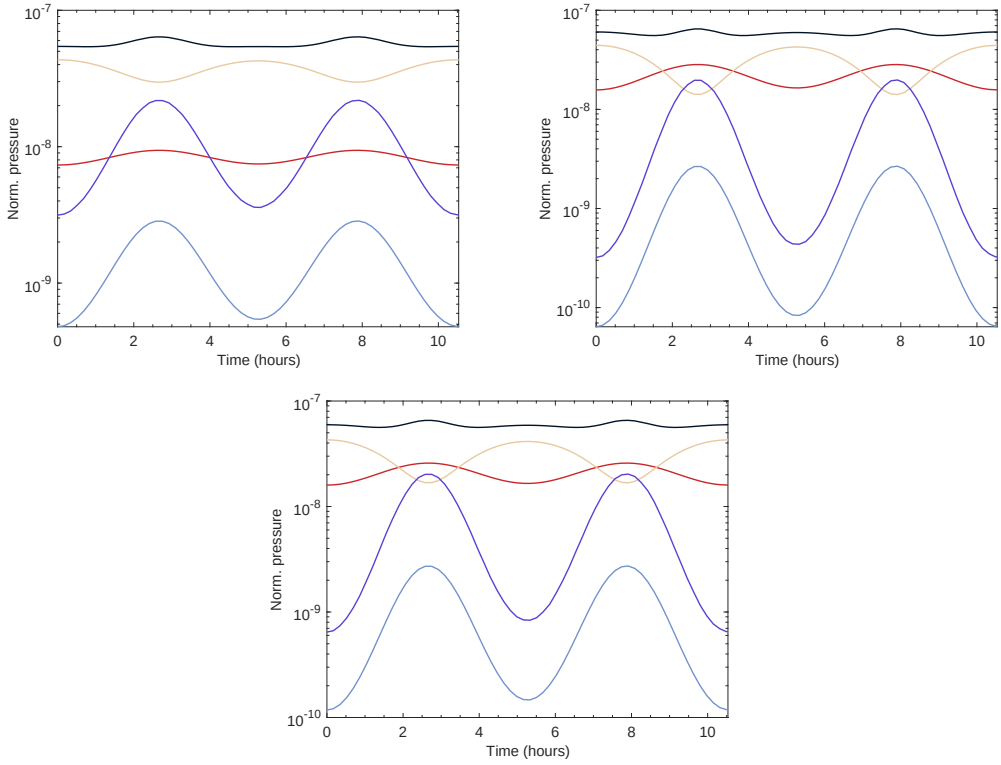

Figure 8. Predictions for the normalised hot (red), cold (blue), dynamic (purple) plasma pressures, magnetic pressure (yellow) and total pressure (black) given by the MDISC model, along Ganymede's orbit, during one synodic period and for different magnetospheric configurations: a compressed configuration (top-left), with $K_h = 1 \times 10^7\,\mathrm{Pa\,m\,T^{-1}}$ and $r_{\max} = 60\,R_J$, an expanded configuration (top-right), with $K_h = 3 \times 10^7\,\mathrm{Pa\,m\,T^{-1}}$ and $r_{\max} = 90\,R_J$, and the optimal PJ34 configuration (bottom), with $K_h = 2.719 \times 10^7\,\mathrm{Pa\,m\,T^{-1}}$ and $r_{\max} = 79.5\,R_J$.

In fact, the cold plasma pressure assumes a much less significant role than the one observed for the Saturnian moon, with the hot pressure becoming the main driver during crossing near Ganymede's orbit. The dynamic pressure also presents as a weaker contribution when compared to Titan's case, where it constitutes the dominant contribution during such events. When over the exterior regions of each respective current sheet, both moons are mostly impacted by the magnetic pressure. Overall, the plasma pressures are shown to be weaker than the ones predicted for Titan during the Cassini flybys analysed by Achilleos et al. (2010), a fact that is compensated by a slight increase in relative intensity of the magnetic pressure particularly during current sheet crossings. The total pressure for the system remains mostly constant, showing a slight increase during crossings, and levels comparable, albeit lower, to the ones predicted near Titan's orbit. It is important to keep in mind that, just like for the case of Ganymede, the plasma environment that surrounds Titan is also influenced by the configuration of Saturn's magnetosphere and, as such, these comparative results refer only to the conditions observed during the particular passes referenced by Achilleos et al. (2010) and using a particular set magnetospheric parameters in order to predict the behaviour of the different pressures. A more detailed comparison between the plasma conditions near both moons could be achieved, in a future study, by first analysing the changes produced by different Saturnian magnetospheric parameters using a similar methodology as the one discussed in this paper.

7 Comparing Juno PJ34 with Galileo Data

We also compare the results given by the Galileo statistical fits with the Juno PJ34 data, as presented in **Figure 9**. These fits are descriptions of a statistical average of magnetometer data, taken over the course of multiple Galileo flybys in the vicinity of Ganymede's orbit, with a maximum height, above or below the magnetic equatorial plane, of $z = 2\,R_J$ and a radial distance range between $12\,R_J$ and $18\,R_J$, as described by Vogt et al. (2022). As such, both the Juno data and magnetodisc predictions shown were restricted to that same domain in order to properly compare them alongside the corresponding fits of statistically-averaged Galileo data. A 60s averaged sampling of the Juno data was also used, despite the narrower radial window of focus, in order to better compare with the average conditions given by the Galileo fits.

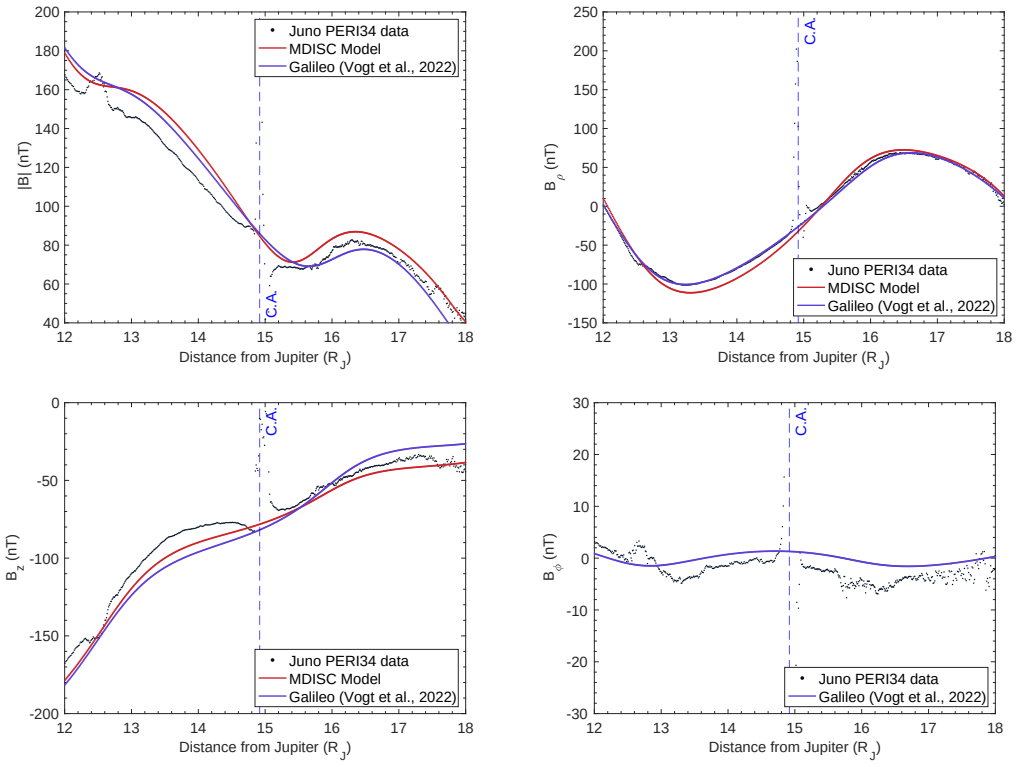

Figure 9. Comparison between the cylindrical components and magnitude of the magnetic field measurements (black), the predicted values by the magnetodisc model (red) and the Galileo data fits (blue), during the portion of the Ganymede encounter that lies within the applicable domain of the Galileo fits, which correspond to a maximum height, above or below the equatorial plane, of $z = 2\,R_J$ and a radial extension range between $12\,R_J$ and $18\,R_J$. Due to the poloidal nature of the field and the absence of radial currents in the magnetodisc model used, no B_ϕ component is given for it.

Both models show reasonable agreement with the field data throughout the encounter with the exception, of course, when sufficiently close to Ganymede. The agreement is particularly good for the radial component of the magnetic field, with the two models producing identical results and fully reproducing the observed behaviour of Jupiter's ambient field before and after the flyby, despite the MDISC model slightly overestimating the radial component of the field. Overall, no significant magnetospheric changes between

the two spacecraft eras can be discerned from these results, thus pointing to somewhat similar conditions. However, this assumption cannot be concluded from this comparison alone and would require a more in-depth analysis of different perijove passes as to determine the extent of such changes. Nevertheless, these results constitute a strong first indicator of the similarity in conditions observed during both spacecraft passes, which may seem particularly interesting due to the large time-frame between Juno orbit PJ34 and the original Galileo observations and dynamic nature of the Jovian magnetosphere, as allowed to by Mauk et al. (1998) during its analysis of the near-Io hot ring current differences observed between Voyager and Galileo eras.

Comparing the predictions given by the MDISC and Galileo models, slight differences become apparent when looking at B_z, where, for distances sufficiently far from the moon, the MDISC model does a better job at capturing the variation in the ambient field. Both models appear to overestimate the intensity of this component of the magnetic field after the encounter with Ganymede, as can also be observed in the magnitude of the field over distances $< 14.8\,R_J$.

8 Conclusions

In this work we have analysed Juno's magnetic field measurements taken during its PJ34 trajectory and compared them with the results predicted by the latest UCL-AGA magnetodisc model. We began by determining the best fitting magnetospheric parameters during the PJ34 trajectory, which consisted of a hot plasma index $K_h = 2.719 \times 10^7\,\mathrm{Pa\,m\,T^{-1}}$ and an effective magnetodisc radius of $r_{\max} = 79.5\,R_J$. Strict confidence intervals were also obtained for each parameter, suggesting that, despite the degenerate nature of their relation, the approach used constitutes a powerful tool for characterising the configuration of Jupiter's magnetosphere and may serve as a motivator for a future analysis on the time-dependence of such parameters.

The optimal fitted parameters were then used in our model in order to predict both the magnetic field and plasma conditions Juno encountered during its trajectory. The results showed good agreement with the in situ measurements throughout the entirety of the trajectory, with the notable exception of the Ganymede flyby, for which our model does not inherently include the contributions coming from all of the moon's magnetospheric fields. However, we added to the existing magnetodisc model a simple dipole field, centred on Ganymede and with an equatorial strength of 719 nT, in order to describe the behaviour of Ganymede's intrinsic field and broadly analyse its influence upon the magnetic environment during the different stages of the flyby. Despite this simple approach, some cases of reasonable agreement were observed. The B_ρ component of the magnetic field generally provided the best agreement between model and observations, whilst a more detailed model description would clearly be needed in order to adequately model the higher order fluctuations observed in the B_z component. Variations in the hot plasma index and effective magnetodisc radius are seen to produce measurable changes in the magnetic field, as shown in the results obtained during the flyby of Ganymede, showing an alteration of up to 33 nT in the field magnitude between a realistically compressed and expanded magnetospheric configuration (Joy et al., 2002). During Juno's encounter with Ganymede, our magnetodisc model's field predictions are generally in alignment with the results obtained by Romanelli et al. (2022), and provide additional context, related to the influence upon field structure of both the Jovian magnetosphere's size and its global hot plasma content.

The model also allowed for a prediction of the plasma environment which Juno encountered during its PJ34 trajectory. During the inbound phase, the hot plasma pressure is shown to provide the maximum pressure during current sheet crossings up to $12\,R_J$, with the magnetic pressure assuming the dominant contribution when closer to the planet. For instances where the spacecraft is in the exterior regions of the current sheet, the hot

and dynamic plasma pressures assume the main role in dictating the pressure environment up to $\sim 12\,R_J$, where the magnetic pressure overpowers them once again. A large variation in intensity for the different plasma pressures is observed between regions along the current sheet and its exterior regions, with this gap becoming much less significant for equatorial distances $> 20\,R_J$ due to a gradual decrease in the relative contribution of the magnetodisc field towards the total equatorial magnetic field, a natural property of the 'disc-like' field generated by the combination of the planet's internal field and the magnetodisc's azimuthal currents, and a change in the spacecraft's trajectory bringing its mean position closer to the magnetic equator.

The outbound phase of the trajectory shows a much more stable pressure behaviour, with the magnetic pressure assuming an overwhelmingly dominant role throughout its entirety, with periodic contributions from the different plasma pressures as the spacecraft weaves in and out of the model's closed field line region of Jupiter's magnetosphere. We also analyse the plasma environment along Ganymede's orbit over one Jovian synodic period, and for different magnetospheric configurations, as summarised by the parameters representing system size and global hot plasma content. As previously observed, during the PJ34 trajectory, the hot, dynamic and cold plasma pressures were shown to vary in anti-phase with the magnetic pressure and achieve maximum values during current sheet crossings. The hot and dynamic plasma pressures are able to surpass the magnetic pressure during such events for the expanded and optimal magnetospheric configurations, while during the compressed scenario, only the hot plasma pressure is able to achieve this effect. The cold plasma pressure was demonstrated to play a much less significant role than the other pressures in dictating the environment near Ganymede's orbit. When compared with the results obtained by Achilleos et al. (2014) through a similar analysis for the case of Titan in the Saturnian system, the plasma pressures are shown to be weaker than those predicted for Titan, with the exception of the magnetic pressure, which shows a slight increase in intensity, particularly during current sheet crossings.

The comparison between the magnetic field measurements taken by Juno during its PJ34 encounter with Ganymede, the predictions provided by our model, the statistical fits of Galileo data taken during multiple flybys in the vicinity of the moon's orbit (Vogt et al., 2022), plausibly indicate somewhat similar magnetospheric configurations at the time of each respective flyby. However, a more detailed analysis incorporating additional perijove datasets would be necessary in order to better the extent and wider influence of these magnetospheric reconfigurations.

Appendix A Determining the Magnetospheric Parameters for PJ34

The full expression for the determination of the chi-square values resulting from the fits is shown in **Equation A1**:

$$\chi^2 = \frac{1}{N-2}\sum_{i=0}^{N}\frac{(B_{\rho M}-B_{\rho J})^2+(B_{zM}-B_{zJ})^2}{\sigma_i^2} \tag{A1}$$

where the M and J subscripts are associated with the field components given by the magnetodisc model and Juno data, respectively, and σ_i was considered constant and approximately equal to the minimum total root-mean square error value of all the sets of magnetospheric parameters fitted ($\sigma = 7.7\,\mathrm{nT}$). The resulting chi-square value was then reduced by dividing it by the number of degrees of freedom, which in this case, given that we fit for a total of two parameters, corresponds to $N-2$, with N being the number of data points used, as shown in **Equation A1**.

A score value, with 1 corresponding to the best fitting, was then attributed to each set based on their probability of matching the observed conditions of the Jovian magnetosphere. This value was determined using the same approach as the one described in Press et al. (1992) and shown in **Equation A2**:

$$Score = 1 - F_{\chi^2}(\Delta\chi^2) = 1 - F_{\chi^2}(\chi^2 - \chi^2_{\min}) \tag{A2}$$

where F_{χ^2} corresponds to the chi-square cumulative distribution function and $\chi^2_{\min}$ to the minimum reduced chi-square obtained in the parameter fitting.

In **Figure A1**, we show the parameter space superposed with a colourmap of the corresponding score associated with each set of magnetospheric parameters. Confidence boundary lines are also shown, each corresponding to the probability that the actual best fitting set of parameters is contained within.

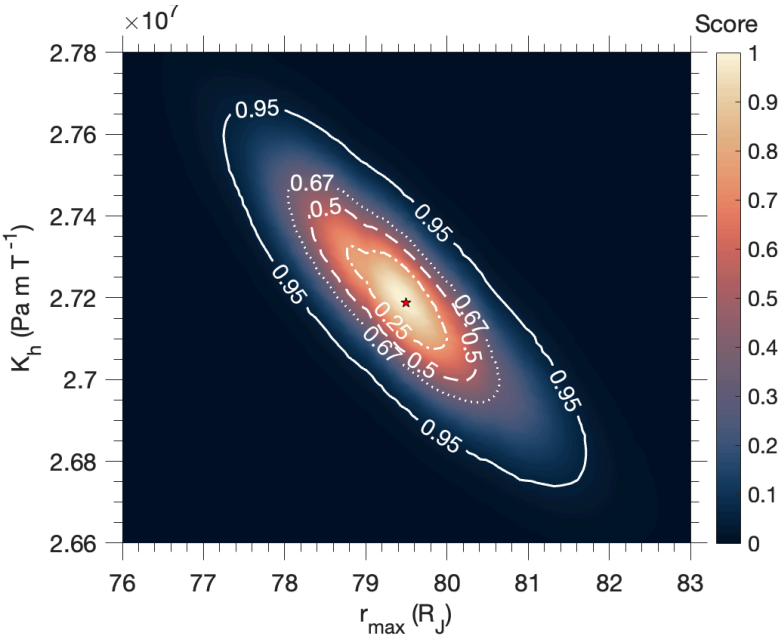

Figure A1. Colour mapping of the magnetospheric parameter space with percentile confidence boundary lines. The nominal best fitting set of parameters is marked with a star.

These results point towards an anticorrelated relationship between the hot plasma index and the effective magnetodisc radius. The ellipsoidal shape of the confidence curves arises from the degenerate nature of this relationship, where a magnetospheric configuration with a higher hot plasma index can result in a similar overarching behaviour as the one produced by an expanded magnetosphere, thus having a higher $r_{\max}$, with a lower K_h value. Looking at the confidence regions, a strict constraint on both magnetospheric parameters can be set for a 95 % confidence level, as shown in **Table A1**, with the parameters only varying up to $\sim$ 4 % and 6 % for K_h and $r_{\max}$, respectively. The best fit being achieved with nominal values of $K_h = 2.719 \times 10^7\,\mathrm{Pa\,m\,T^{-1}}$ and $r_{\max} = 79.5\,R_J$ for the two parameters, respectively.

It is important to note that the results shown are dependent on the tilt angle θ_d and reference jovigraphic longitude ϕ_d of Jupiter's magnetic dipole used to project the PJ34 position and magnetic field data onto the jovimagnetic reference frame, which in

Table A1. Confidence interval boundaries for each magnetospheric parameter when fitting the Juno PJ34 data, with their values corresponding to the horizontal and vertical extents of the ellipse for each respective confidence level.

Confidence level	Hot plasma index K_h ($\mathrm{Pa\,m\,T^{-1}}$)	Effective magnetodisc radius $r_{\max}$ (R_J)
95 %	$[2.674 \times 10^7, 2.768 \times 10^7]$	[77.3, 81.7]
67 %	$[2.694 \times 10^7, 2.750 \times 10^7]$	[78.1, 80.7]
50 %	$[2.699 \times 10^7, 2.744 \times 10^7]$	[78.3, 80.4]
25 %	$[2.708 \times 10^7, 2.733 \times 10^7]$	[78.8, 80.0]
Optimal values	2.719×10^7	79.5

turn allows for a direct comparison with the model's predictions. During this study, we utilise the same $\theta_d = 10.31°$ and $\phi_d = 163.39°$ obtained by Connerney et al. (2018) and used by Vogt et al. (2022). The impact of different values for these two quantities in the determination of best fitting magnetospheric parameters was also analysed, using both the angles obtained by Connerney et al. (1998) ($\theta_d = 9.5°$; $\phi_d = 159.2°$) and Connerney et al. (2022) ($\theta_d = 10.25°$; $\phi_d = 163.62°$). The results pertaining to the former produced statistically significant changes in the optimal values of these parameters when compared to the results shown in **Table A1**, with values being within 8σ and 4σ for K_h and $r_{\max}$, respectively. However, this discrepancy can be explained by the considerable change in both the values of θ_d and ϕ_d between the publications of Connerney et al. (1998) and Connerney et al. (2018), a consequence of the remarkable progress made possible by Juno measurements taken during its first nine orbits around Jupiter. This hypothesis is further supported by the results obtained using the latest set of angles reported by Connerney et al. (2022), which are in full agreement with the ones shown in **Table A1**, with optimal K_h remaining unchanged and $r_{\max}$ within $< 1\sigma$.

Appendix B Data Availability Statement

The magnetic field and positional data related to Juno's PJ34 trajectory can be downloaded from `https://pds-ppi.igpp.ucla.edu/search/?sc=Juno&t=Jupiter&i=FGM`, while the data pertaining to the magnetospheric parameter estimation is available at `https://github.com/AlexFdSantos/PJ34MagPlasma`.

Acknowledgments

A.S. was supported by the UK Science and Technology Facilities Council (STFC) through a PhD studentship, hosted by the UCL Department of Physics and Astronomy.

References

Achilleos, N., Arridge, C. S., Bertucci, C., Guio, P., Romanelli, N., & Sergis, N. (2014, December). A combined model of pressure variations in Titan's plasma environment. *Geophysical Research Letters*, *41*(24), 8730-8735. doi: 10.1002/2014GL061747

Achilleos, N., Guio, P., & Arridge, C. S. (2010, February). A model of force balance in Saturn's magnetodisc. *Monthly Notices of the Royal Astronomical Society*, *401*(4), 2349-2371. doi: 10.1111/j.1365-2966.2009.15865.x

Bunce, E. J., Cowley, S. W. H., Alexeev, I. I., Arridge, C. S., Dougherty, M. K., Nichols, J. D., & Russell, C. T. (2007, October). Cassini observations of the

variation of saturn's ring current parameters with system size. *Journal of Geophysical Research: Space Physics*, *112*(A10). doi: https://doi.org/10.1029/2007JA012275

Caudal, G. (1986, April). A SELF-CONSISTENT MODEL OF JUPITER'S MAGNETODISC INCLUDING THE EFFECTS OF CENTRIFUGAL FORCE AND PRESSURE. *Journal of Geophysical Research*, *91*(A4), 4201-4221. doi: 10.1029/JA091iA04p04201

Connerney, J. E. P., Acuña, M. H., & Ness, N. F. (1982, May). Voyager 1 assessment of Jupiter's planetary magnetic field. *Journal of Geophysical Research (Space Physics)*, *87*(A5), 3623-3627. doi: https://doi.org/10.1029/JA087iA05p03623

Connerney, J. E. P., Acuña, M. H., Ness, N. F., & Satoh, T. (1998, June). New models of jupiter's magnetic field constrained by the io flux tube footprint. *Journal of Geophysical Research: Space Physics*, *103*(A6), 11929-11939. doi: https://doi.org/10.1029/97JA03726

Connerney, J. E. P., Adriani, A., Allegrini, F., Bagenal, F., Bolton, S. J., Bonfond, B., ... Waite, J. (2017, May). Jupiter's magnetosphere and aurorae observed by the Juno spacecraft during its first polar orbits. *Science*, *356*(6340), 826-832. doi: 10.1126/science.aam5928

Connerney, J. E. P., Benn, M., Bjarno, J. B., Denver, T., Espley, J., Jorgensen, J. L., ... Smith, E. J. (2017, November). The Juno Magnetic Field Investigation. *Space Science Reviews*, *213*(1-4), 39-138. doi: 10.1007/s11214-017-0334-z

Connerney, J. E. P., Kotsiaros, S., Oliversen, R. J., Espley, J. R., Joergensen, J. L., Joergensen, P. S., ... Levin, S. M. (2018, March). A new model of jupiter's magnetic field from juno's first nine orbits. *Geophysical Research Letters*, *45*(6), 2590-2596. doi: https://doi.org/10.1002/2018GL077312

Connerney, J. E. P., Timmins, S., Oliversen, R. J., Espley, J. R., Joergensen, J. L., Kotsiaros, S., ... Levin, S. M. (2022, February). A New Model of Jupiter's Magnetic Field at the Completion of Juno's Prime Mission. *Journal of Geophysical Research (Planets)*, *127*(2), e2021JE007055. doi: 10.1029/2021JE007055

Ferraro, V. C. A. (1937, April). The non-uniform rotation of the sun and its magnetic field. *Monthly Notices of the Royal Astronomical Society*, *97*, 458. doi: 10.1093/mnras/97.6.458

Gledhill, J. A. (1967, April). Magnetosphere of Jupiter. *Nature*, *214*(5084), 155-156. doi: 10.1038/214155a0

Hill, T. (1979). Inertial limit on corotation. *Journal of Geophysical Research: Space Physics*, *84*(A11), 6554-6558. doi: 10.1029/JA084iA11p06554

Jacobson, R. (2014, April). The Orbits of the Regular Jovian Satellites. In *European planetary science congress* (Vol. 9, p. EPSC2014-73).

Jia, X., & Kivelson, M. G. (2021, April). The magnetosphere of ganymede. In *Magnetospheres in the solar system* (p. 557-573). American Geophysical Union (AGU). doi: https://doi.org/10.1002/9781119815624.ch35

Jia, X., Walker, R. J., Kivelson, M. G., Khurana, K. K., & Linker, J. A. (2008, June). Three-dimensional mhd simulations of ganymede's magnetosphere. *Journal of Geophysical Research: Space Physics*, *113*(A6). doi: https://doi.org/10.1029/2007JA012748

Joy, S. P., Kivelson, M. G., Walker, R. J., Khurana, K. K., Russell, C. T., & Ogino, T. (2002, October). Probabilistic models of the Jovian magnetopause and bow shock locations. *Journal of Geophysical Research (Space Physics)*, *107*(A10), 1309. doi: 10.1029/2001JA009146

Kaweeyanun, N., Masters, A., & Jia, X. (2020, March). Favorable conditions for magnetic reconnection at ganymede's upstream magnetopause. *Geophysical Research Letters*, *47*(6), e2019GL086228. doi: https://doi.org/10.1029/

2019GL086228

Khurana, K. K. (1997, June). Euler potential models of jupiter's magnetospheric field. *Journal of Geophysical Research: Space Physics*, *102*(A6), 11295-11306. doi: 10.1029/97JA00563

Khurana, K. K., & Kivelson, M. G. (1993, January). Inference of the angular velocity of plasma in the jovian magnetosphere from the sweepback of magnetic field. *Journal of Geophysical Research: Space Physics*, *98*(A1), 67-79. doi: https://doi.org/10.1029/92JA01890

Kivelson, M. G., Khurana, K. K., Russell, C. T., Walker, R. J., Coleman, P. J., Coroniti, F. V., ... Huddleston, D. E. (1997, January). Galileo at Jupiter: Changing states of the magnetosphere and first looks at Io and Ganymede. *Advances in Space Research*, *20*(2), 193-204. (Planetary Ionospheres and Magnetospheres) doi: https://doi.org/10.1016/S0273-1177(97)00533-4

Kivelson, M. G., Khurana, K. K., & Volwerk, M. (2002, June). The Permanent and Inductive Magnetic Moments of Ganymede. *Icarus*, *157*(2), 507-522. doi: https://doi.org/10.1006/icar.2002.6834

Mauk, B. H., McEntire, R. W., Williams, D. J., Lagg, A., Roelof, E. C., Krimigis, S. M., ... Wilken, B. (1998, March). Galileo-measured depletion of near-io hot ring current plasmas since the voyager epoch. *Journal of Geophysical Research: Space Physics*, *103*(A3), 4715-4722. doi: https://doi.org/10.1029/97JA02343

Millas, D., Achilleos, N., Guio, P., & Arridge, C. S. (2023, January). Modelling magnetic fields and plasma flows in the magnetosphere of Jupiter. *Planetary and Space Science*, *225*(105609). doi: 10.1016/j.pss.2022.105609

Nichols, J. D., Achilleos, N., & Cowley, S. W. H. (2015, December). A model of force balance in Jupiter's magnetodisc including hot plasma pressure anisotropy. *Journal of Geophysical Research (Space Physics)*, *120*(12), 10,185-10,206. doi: 10.1002/2015JA021807

Pontius, D. H. (1997, April). Radial mass transport and rotational dynamics. *Journal of Geophysical Research (Space Physics)*, *102*(A4), 7137-7150. doi: 10.1029/97JA00289

Press, W. H., Teukolsky, S. A., Vetterling, W. T., & Flannery, B. P. (1992). *Numerical Recipes in C - The Art of Scientific Computing* (Second ed.). Cambridge University Press.

Romanelli, N., DiBraccio, G. A., Modolo, R., Connerney, J. E. P., Ebert, R. W., Martos, Y. M., ... Bolton, S. J. (2022, December). Juno Magnetometer Observations at Ganymede: Comparisons With a Global Hybrid Simulation and Indications of Magnetopause Reconnection. *Geophysical Research Letters*, *49*(23), e2022GL099545. doi: 10.1029/2022GL099545

Saur, J., Duling, S., Roth, L., Jia, X., Strobel, D. F., Feldman, P. D., ... Hartkorn, O. (2015, February). The search for a subsurface ocean in ganymede with hubble space telescope observations of its auroral ovals. *Journal of Geophysical Research: Space Physics*, *120*(3), 1715-1737. doi: https://doi.org/10.1002/2014JA020778

Simpson, J. A., Hamilton, D., Lentz, G., McKibben, R. B., Mogro-Campero, A., Perkins, M., ... O'Gallagher, J. J. (1974, January). Protons and Electrons in Jupiter's Magnetic Field: Results from the University of Chicago Experiment on Pioneer 10. *Science*, *183*(4122), 306-309. doi: 10.1126/science.183.4122.306

Smith, E. J., Davis, L., Jones, D. E., Coleman, P. J., Colburn, D. S., Dyal, P., & Sonett, C. P. (1975). Jupiter's magnetic field, magnetosphere, and interaction with the solar wind: Pioneer 11. *Science*, *188*(4187), 451–455.

Sorba, A. M., Achilleos, N. A., Sergis, N., Guio, P., Arridge, C. S., & Dougherty, M. K. (2019, July). Local time variation in the large-scale structure of saturn's magnetosphere. *Journal of Geophysical Research: Space Physics*, *124*(9), 7425-7441. doi: https://doi.org/10.1029/2018JA026363

Stone, S. M., & Armstrong, T. P. (2001, October). Three-dimensional magnetopause and tail current model of the magnetosphere of ganymede. *Journal of Geophysical Research: Space Physics*, *106*(A10), 21263-21275. doi: https://doi.org/10.1029/2000JA000313

Vogt, M. F., Bagenal, F., & Bolton, S. J. (2022, December). Magnetic Field Conditions Upstream of Ganymede. *Journal of Geophysical Research (Space Physics)*, *127*(12), e2022JA030497. doi: 10.1029/2022JA030497

Zimmer, C., Khurana, K. K., & Kivelson, M. G. (2000, October). Subsurface Oceans on Europa and Callisto: Constraints from Galileo Magnetometer Observations. *Icarus*, *147*(2), 329-347. doi: 10.1006/icar.2000.6456

Figure 1.

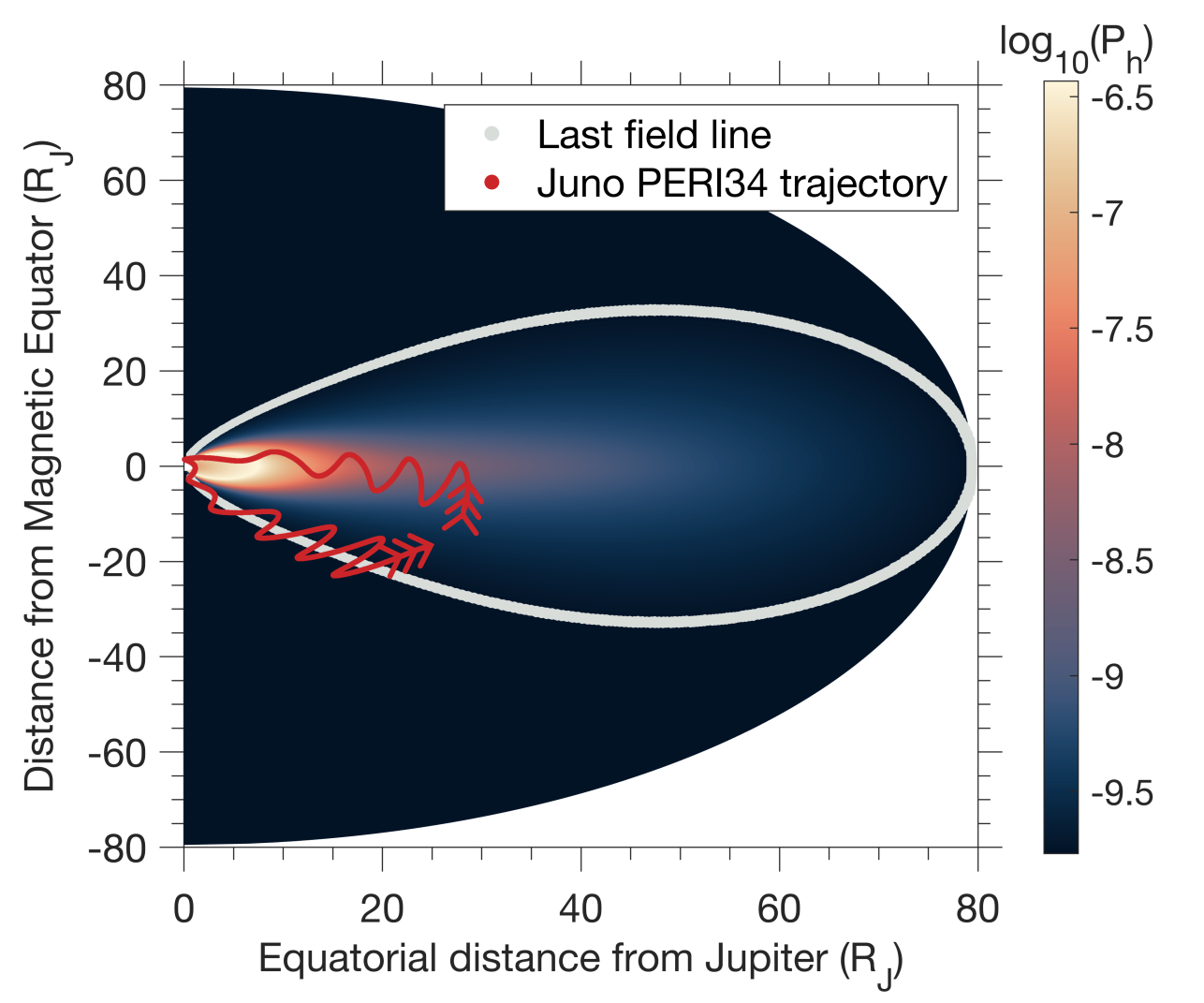
log10(Ph)
-6.5
-7
-7.5
-8
-8.5
-9
-9.5
Last field line
Juno PERI34 trajectory
Distance from Magnetic Equator (RJ)
80
60
40
20
0
-20
-40
-60
-80
0
20
40
60
80
Equatorial distance from Jupiter (RJ)

Figure 2.

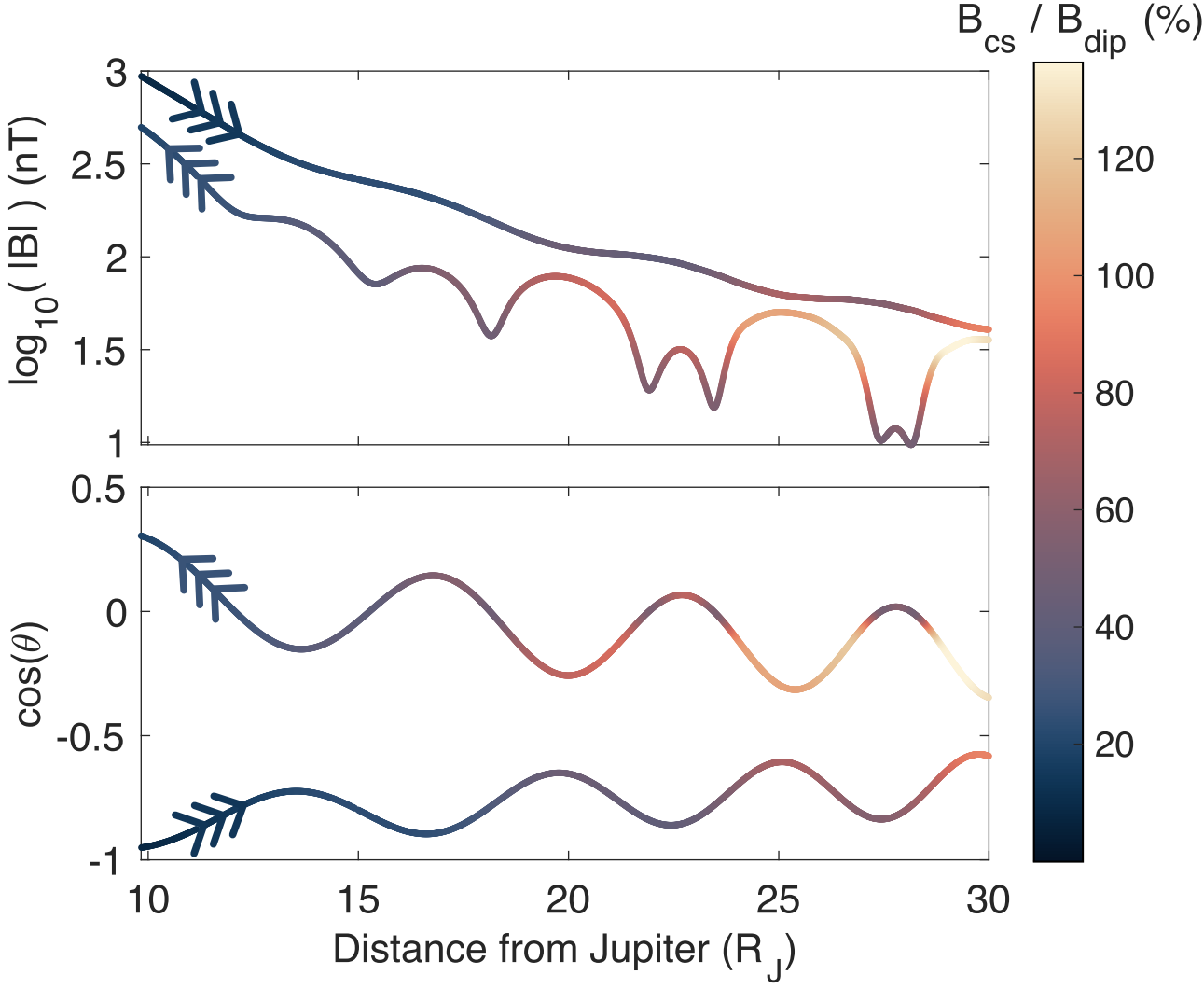
B_cs / B_dip (%)
120
100
80
60
40
20
log10(IBI) (nT)
3
2.5
2
1.5
1
cos(θ)
0.5
0
-0.5
-1
10
15
20
25
30
Distance from Jupiter (R_J)

Figure 3.

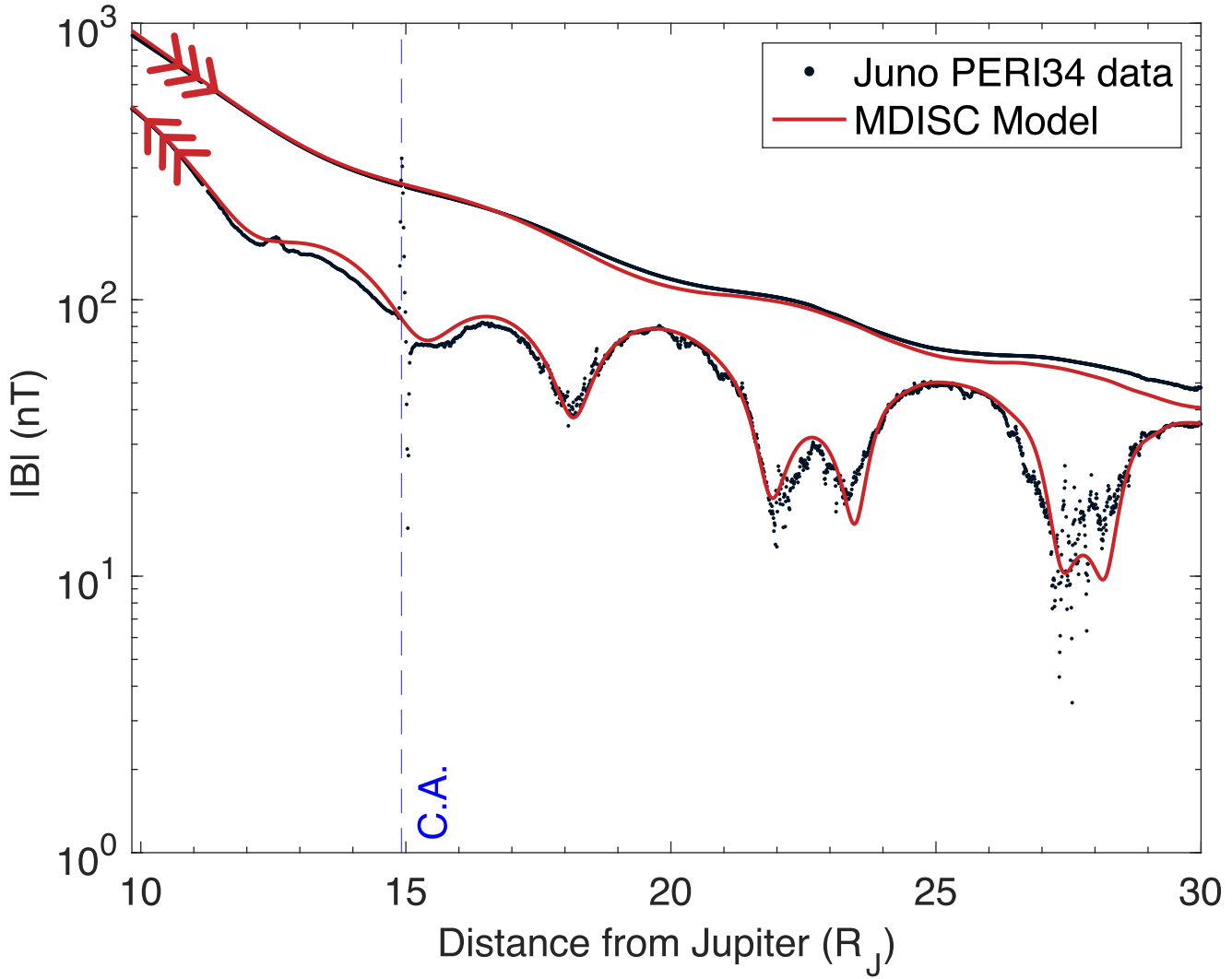
Juno PERI34 data
MDISC Model
C.A.
|B| (nT)
Distance from Jupiter (R_J)
10^3
10^2
10^1
10^0
10
15
20
25
30

Figure 3.

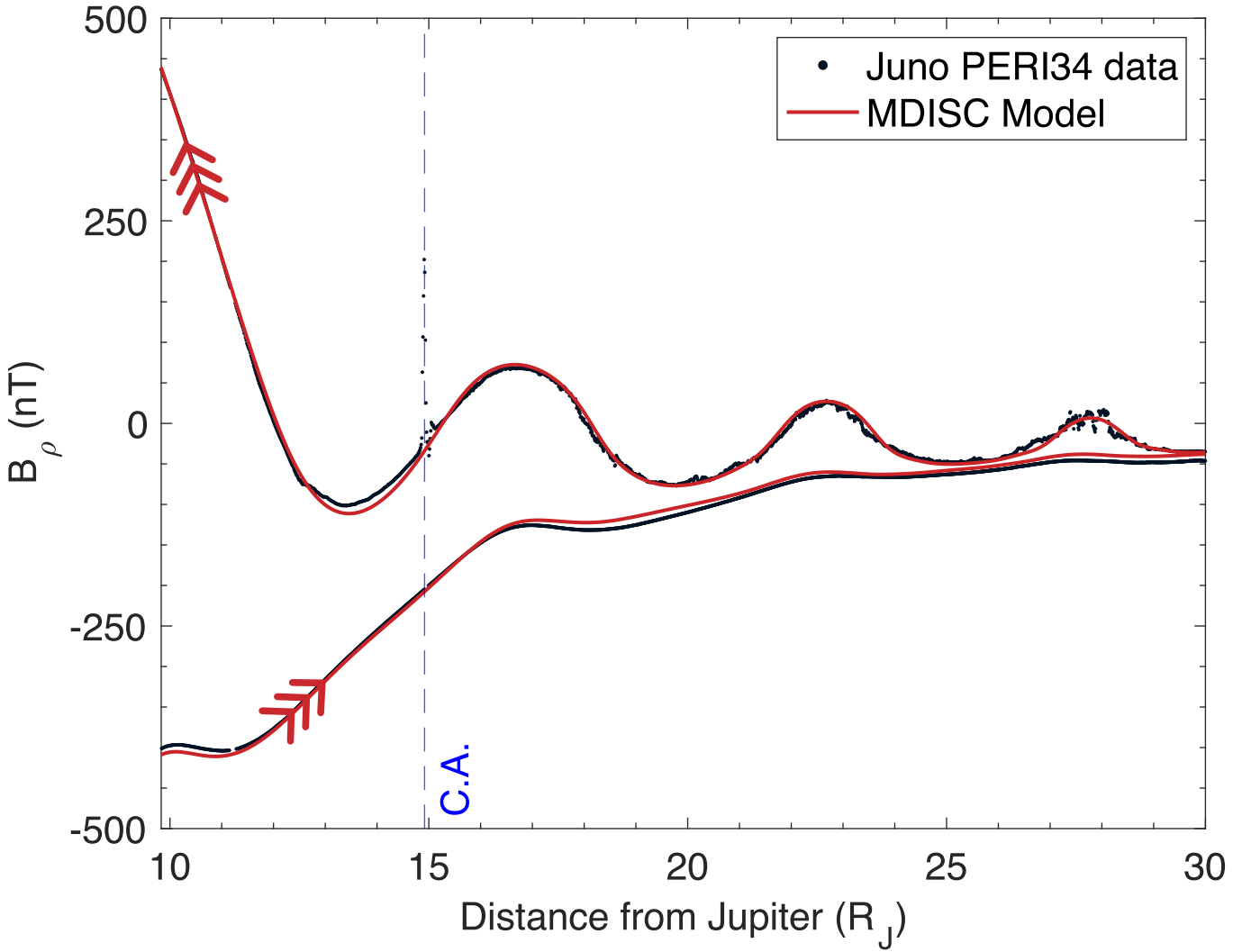
Juno PERI34 data
MDISC Model
C.A.
500
250
0
-250
-500
10
15
20
25
30
B ρ (nT)
Distance from Jupiter (R J)

Figure 3.

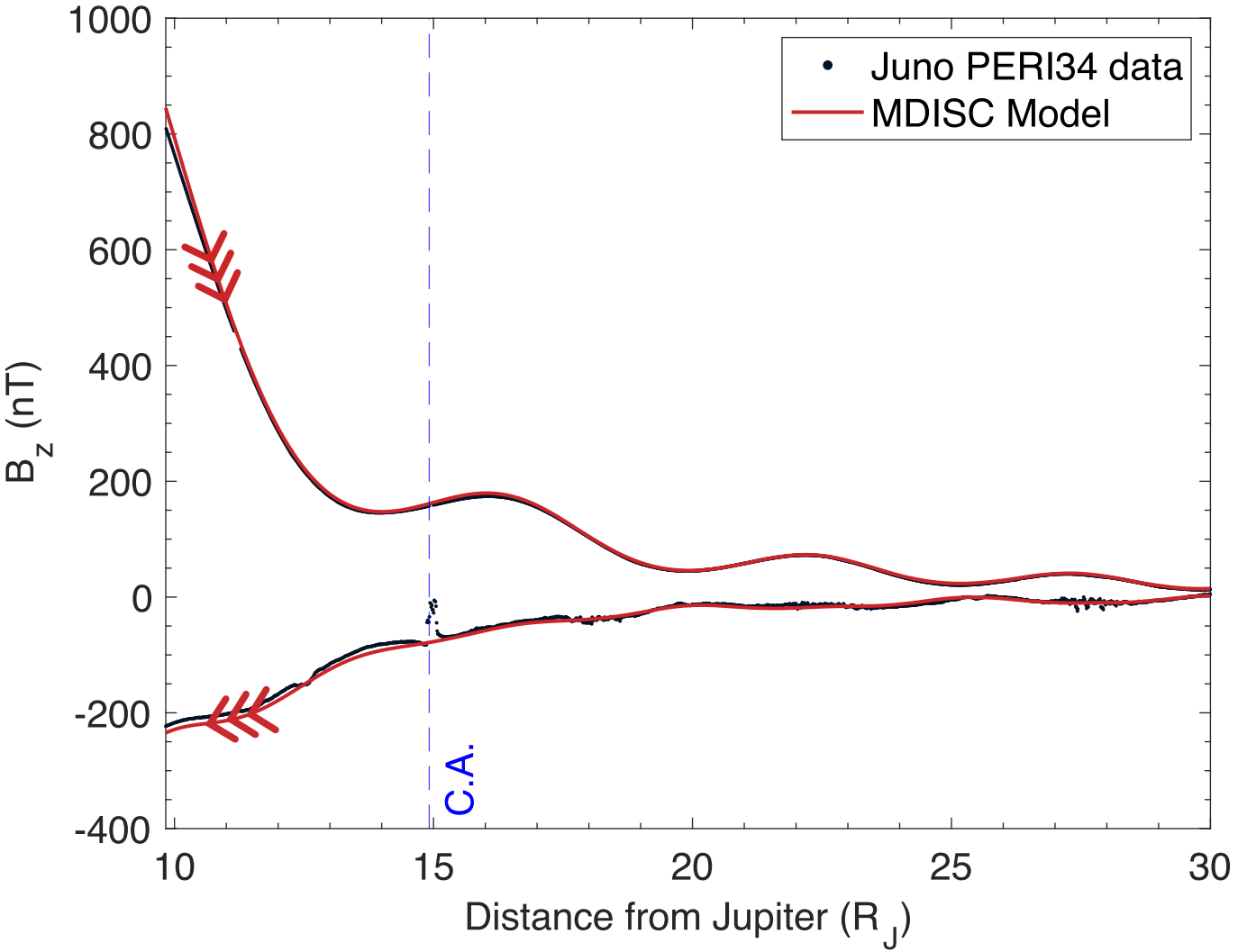
Juno PERI34 data
MDISC Model
C.A.
B_z (nT)
Distance from Jupiter (R_J)
1000
800
600
400
200
0
-200
-400
10
15
20
25
30

Figure 3.

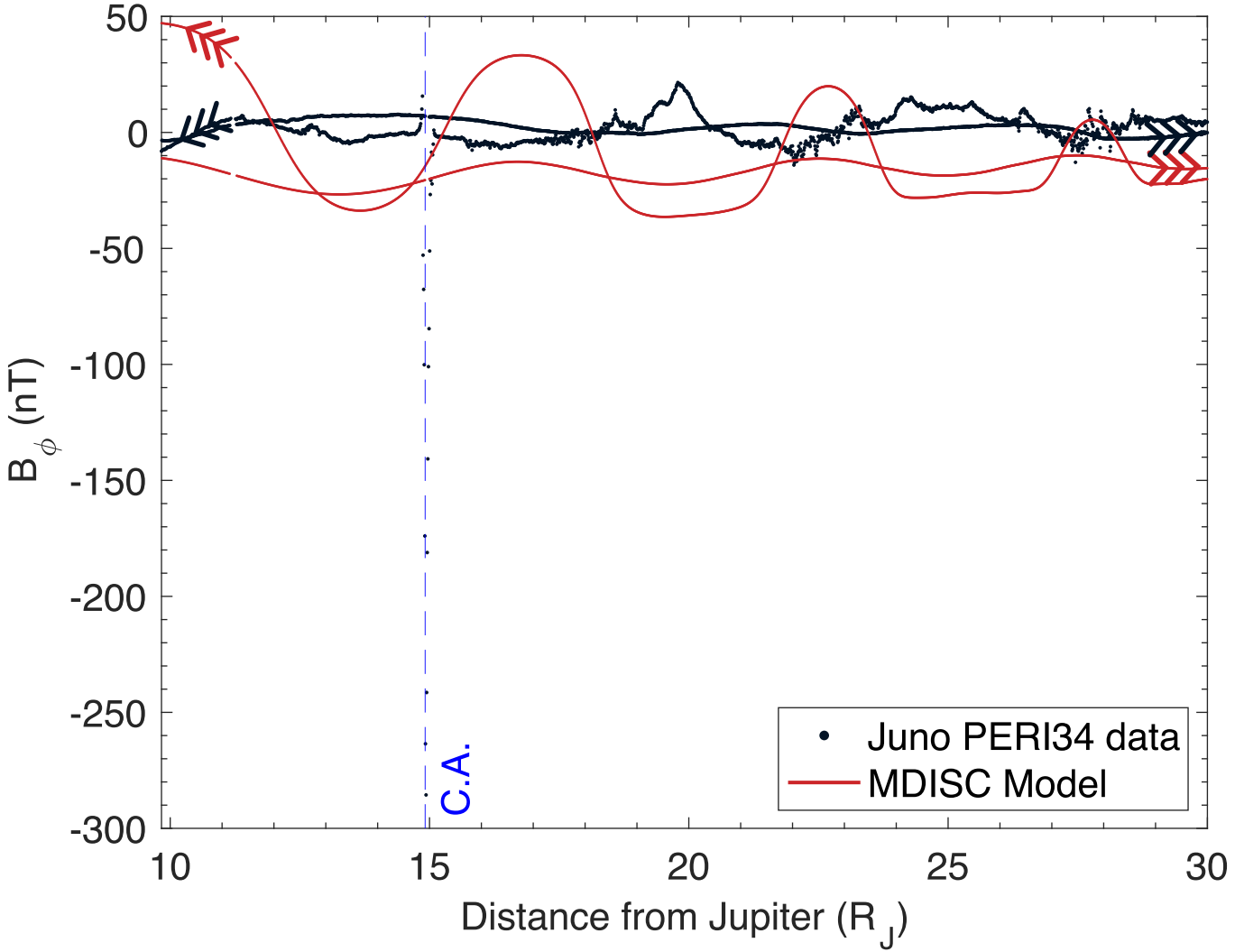
50
0
-50
-100
-150
-200
-250
-300
B_ϕ (nT)
10
15
20
25
30
Distance from Jupiter (R_J)
C.A.
Juno PERI34 data
MDISC Model

Figure 4.

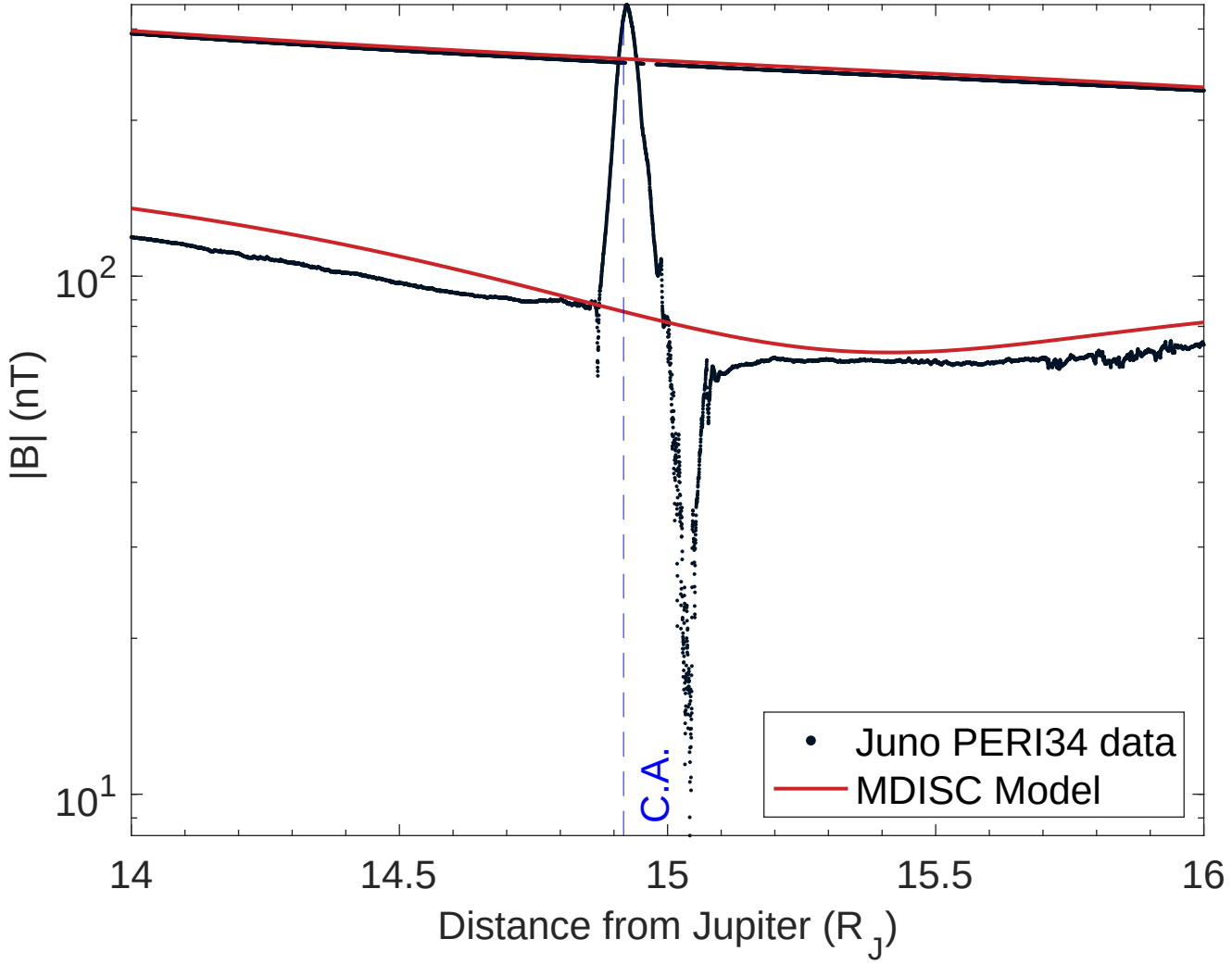
|B| (nT)
10^2
10^1
14
14.5
15
15.5
16
Distance from Jupiter (R_J)
C.A.
Juno PERI34 data
MDISC Model

Figure 4.

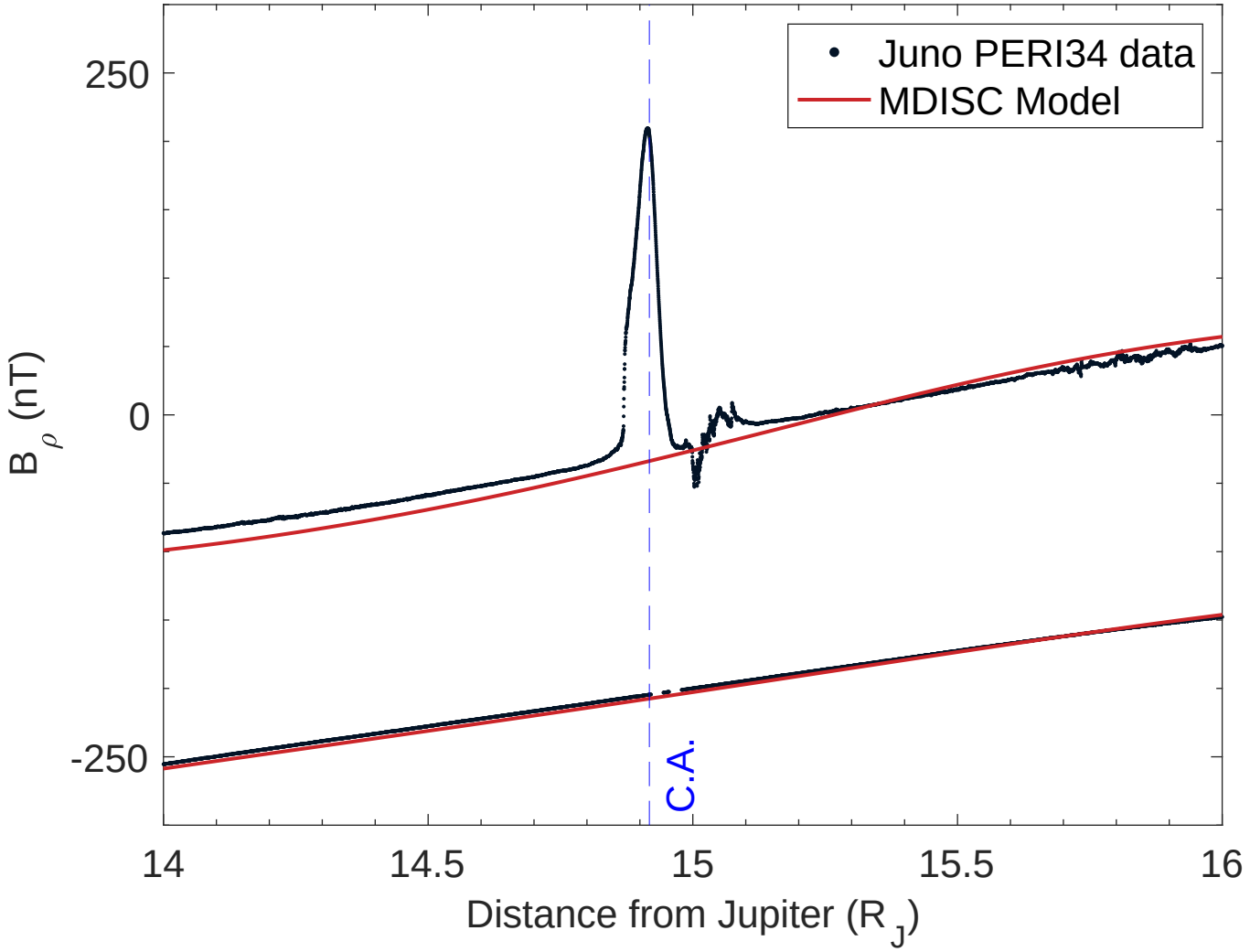
Juno PERI34 data
MDISC Model
250
0
-250
B $_\rho$ (nT)
C.A.
14
14.5
15
15.5
16
Distance from Jupiter (R $_J$)

Figure 4.

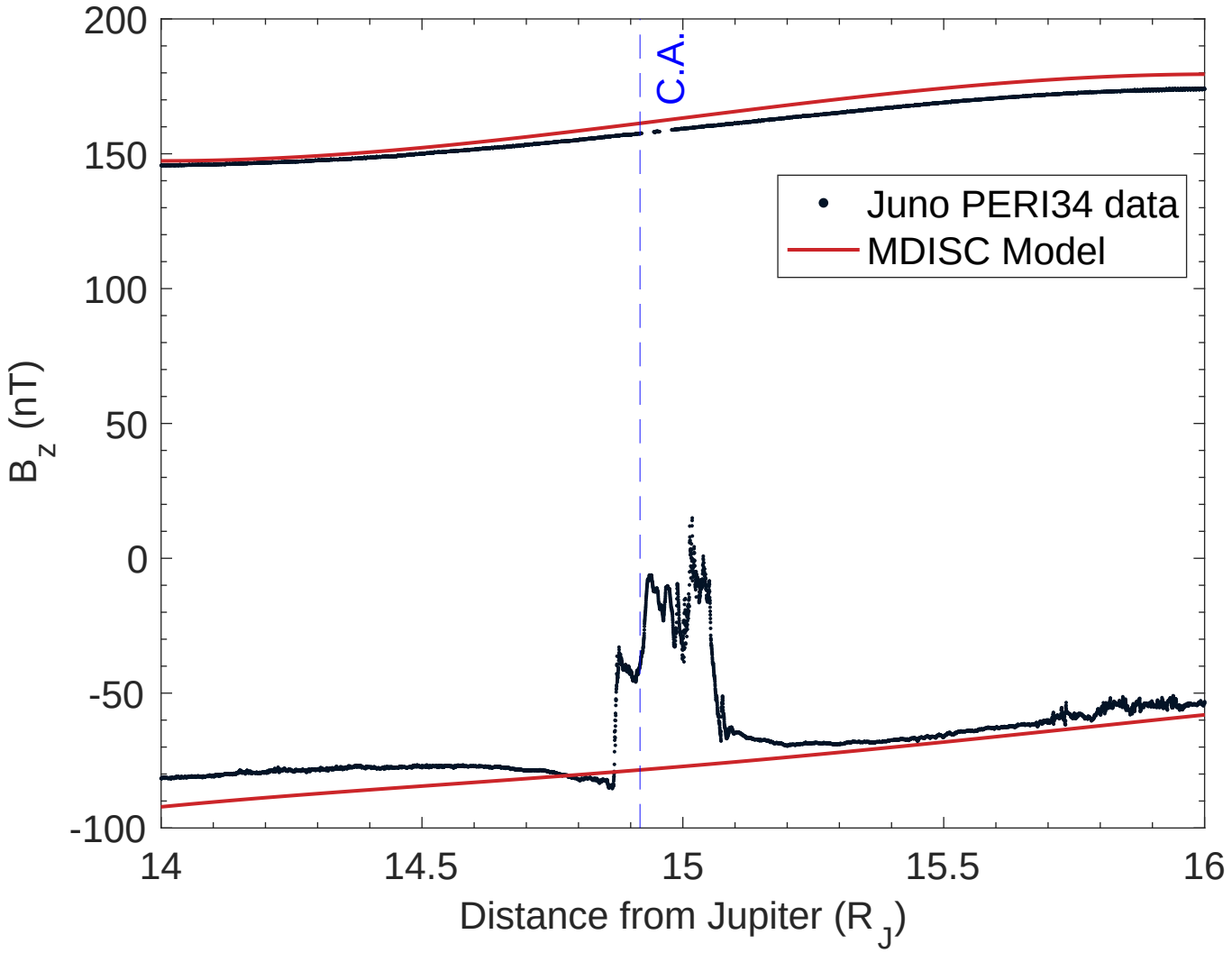
200
150
100
50
0
-50
-100
14
14.5
15
15.5
16
C.A.
Juno PERI34 data
MDISC Model
B_z (nT)
Distance from Jupiter (R_J)

Figure 5.

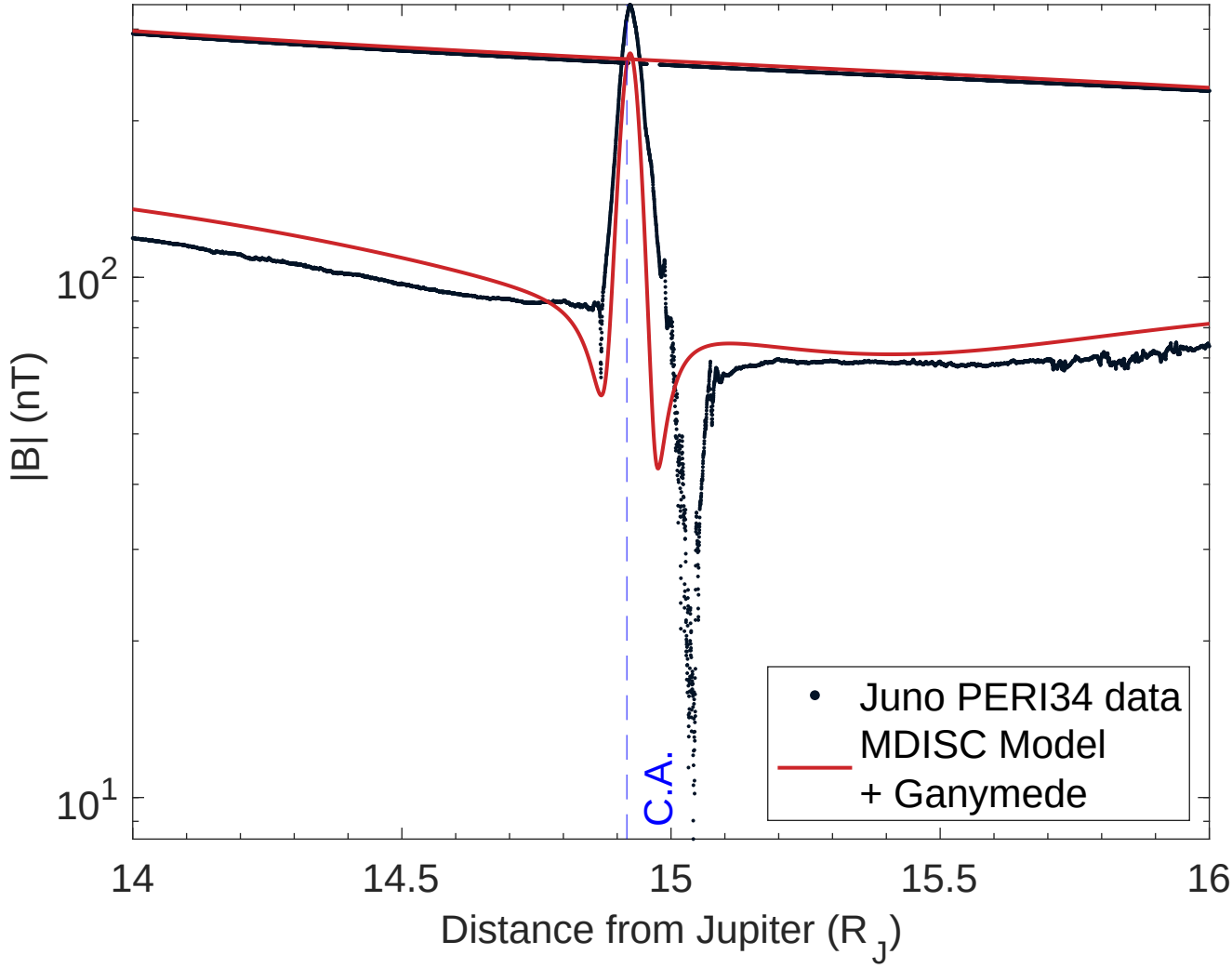
|B| (nT)
10^2
10^1
14
14.5
15
15.5
16
Distance from Jupiter (R_J)
C.A.
Juno PERI34 data
MDISC Model
+ Ganymede

Figure 5.

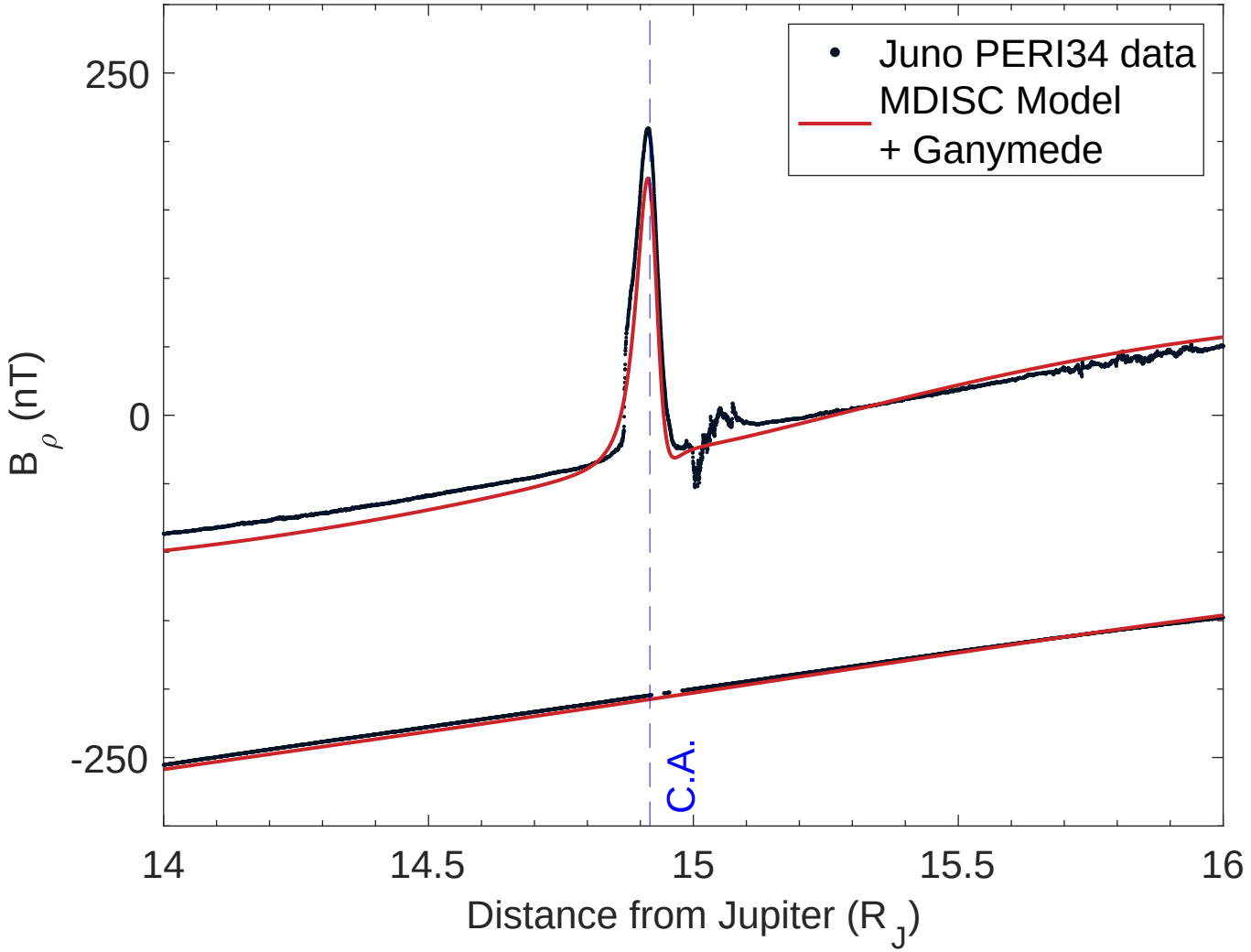
Juno PERI34 data
MDISC Model
+ Ganymede
250
0
-250
B ρ (nT)
C.A.
14
14.5
15
15.5
16
Distance from Jupiter (R J)

Figure 5.

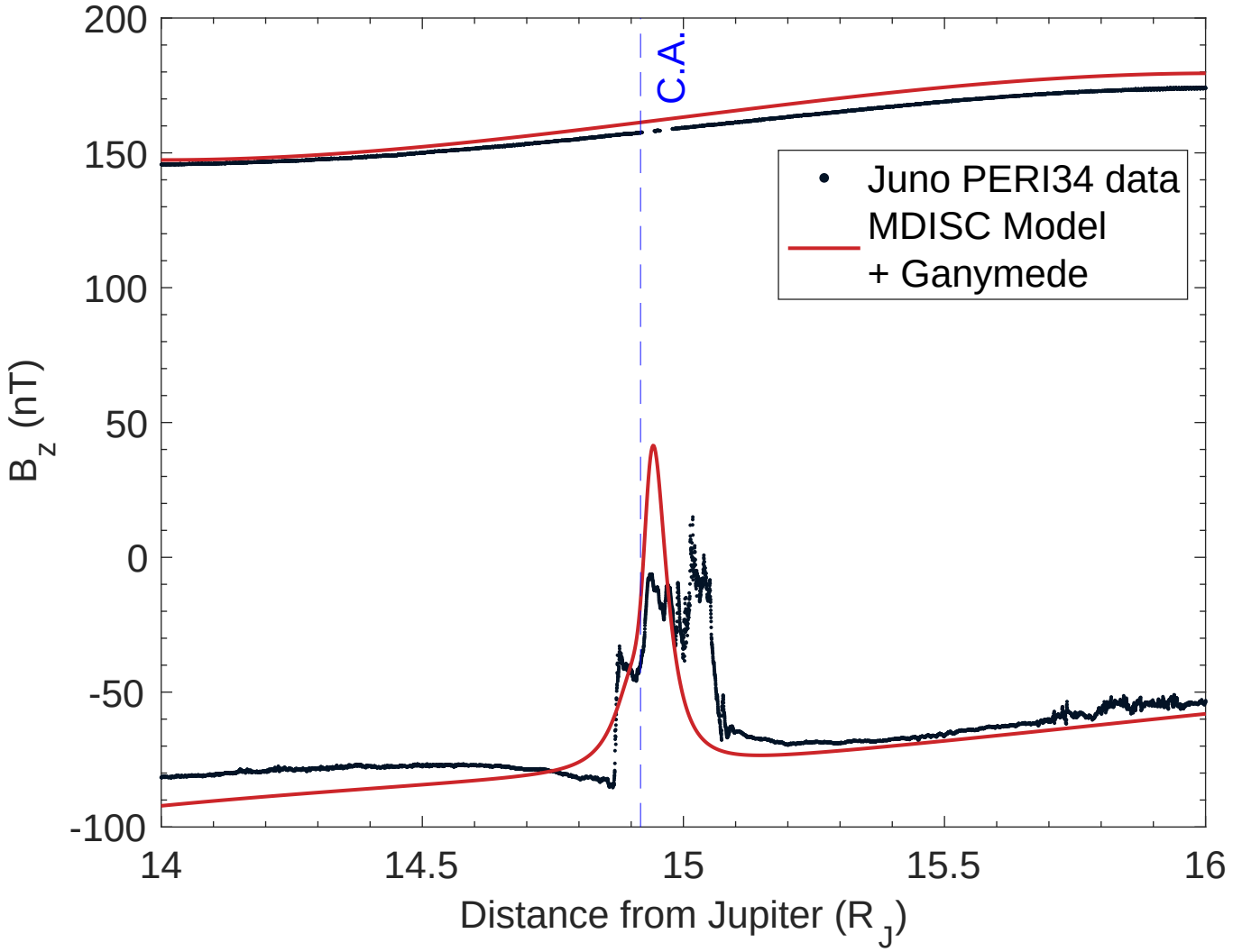
200
150
100
50
0
-50
-100
14
14.5
15
15.5
16
C.A.
Juno PERI34 data
MDISC Model
+ Ganymede
B_z (nT)
Distance from Jupiter (R_J)

Figure 6.

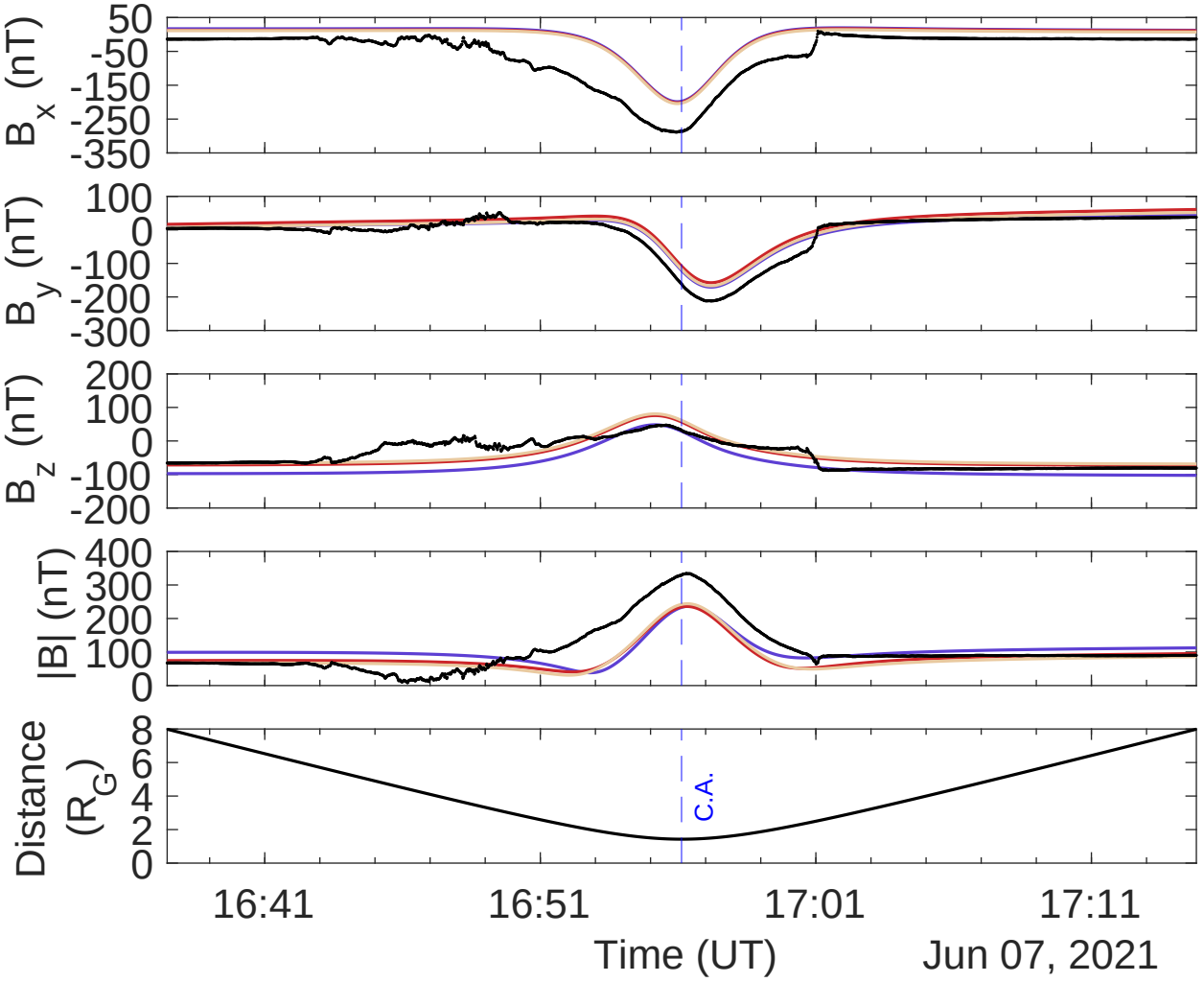
B_x (nT)
50
-50
-150
-250
-350
B_y (nT)
100
0
-100
-200
-300
B_z (nT)
200
100
0
-100
-200
|B| (nT)
400
300
200
100
0
Distance (R_G)
8
6
4
2
0
C.A.
16:41
16:51
17:01
17:11
Time (UT)
Jun 07, 2021

Figure 7.

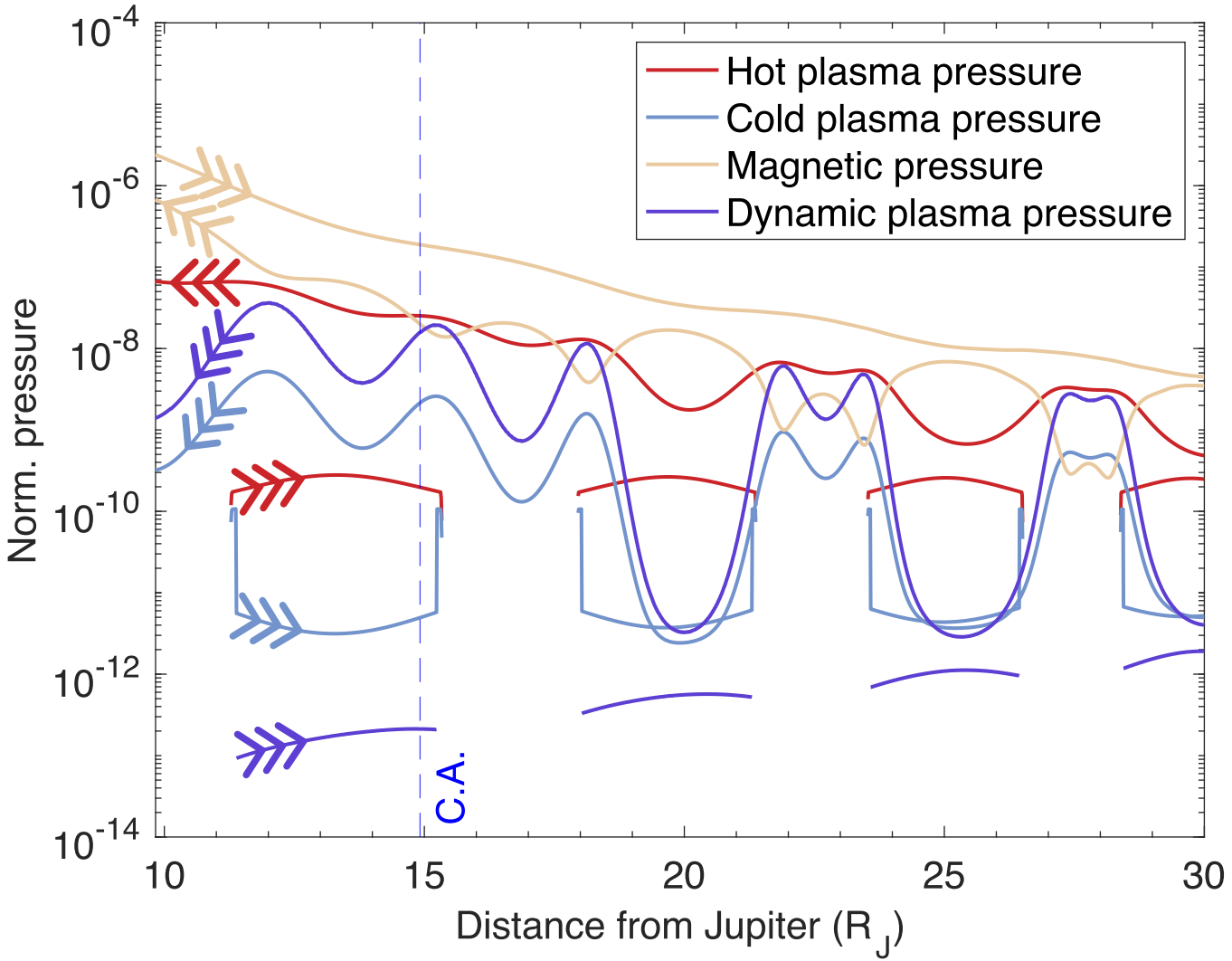
Hot plasma pressure
Cold plasma pressure
Magnetic pressure
Dynamic plasma pressure
C.A.
Norm. pressure
Distance from Jupiter (R J)
10^-4
10^-6
10^-8
10^-10
10^-12
10^-14
10
15
20
25
30

Figure 8.

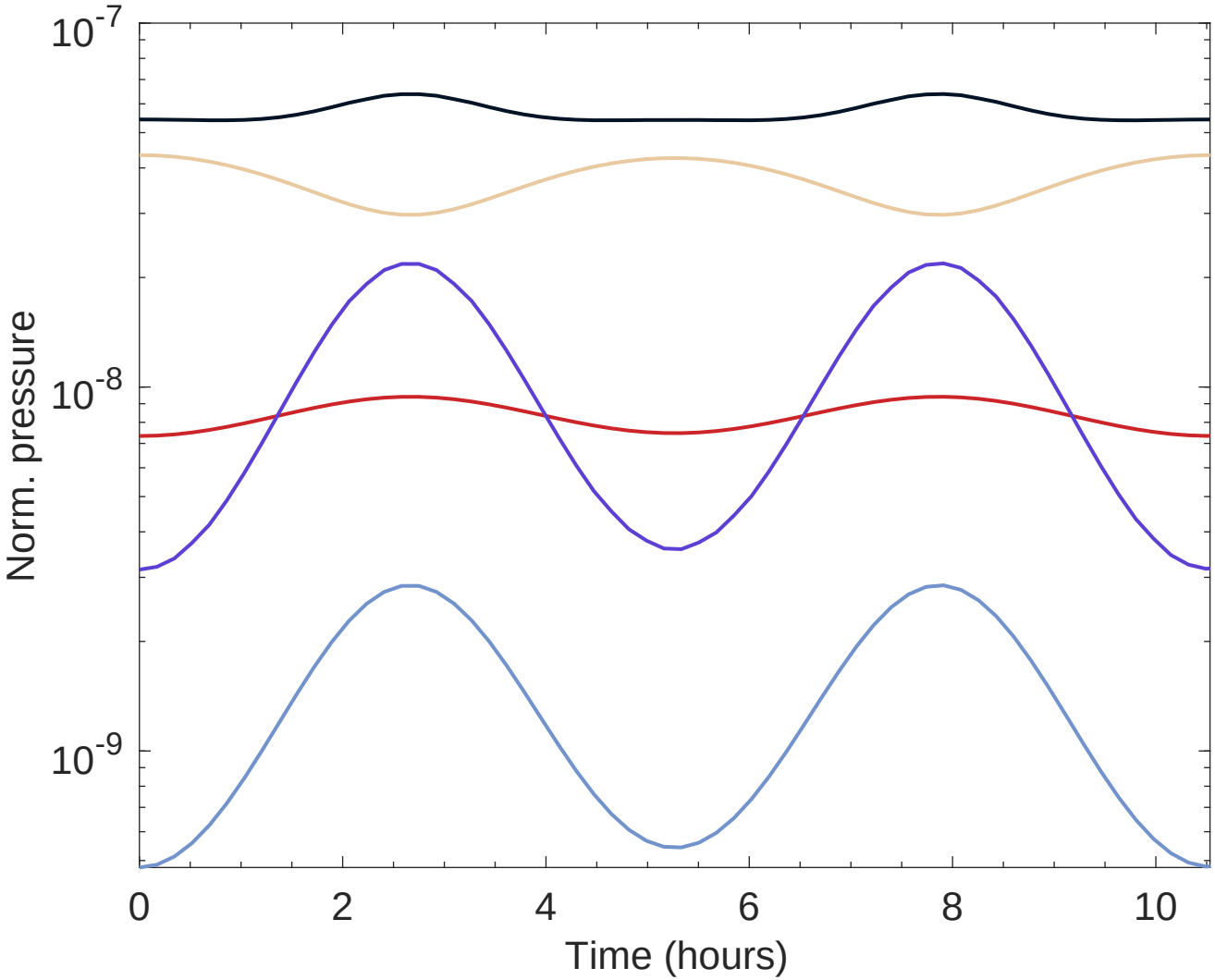
10^-7
10^-8
10^-9
Norm. pressure
0
2
4
6
8
10
Time (hours)

Figure 8.

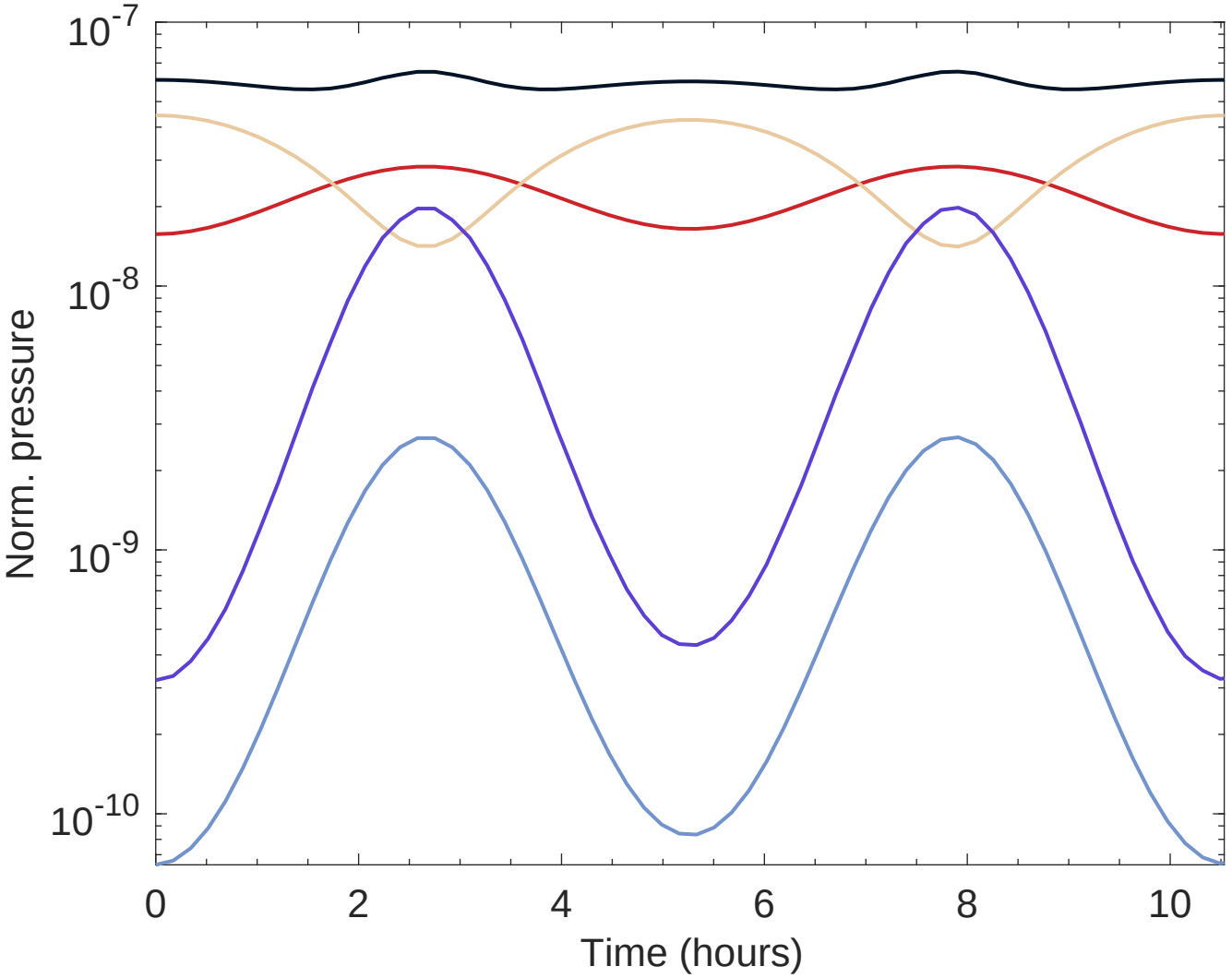
10^{-7}
10^{-8}
10^{-9}
10^{-10}
Norm. pressure
0
2
4
6
8
10
Time (hours)

Figure 8.

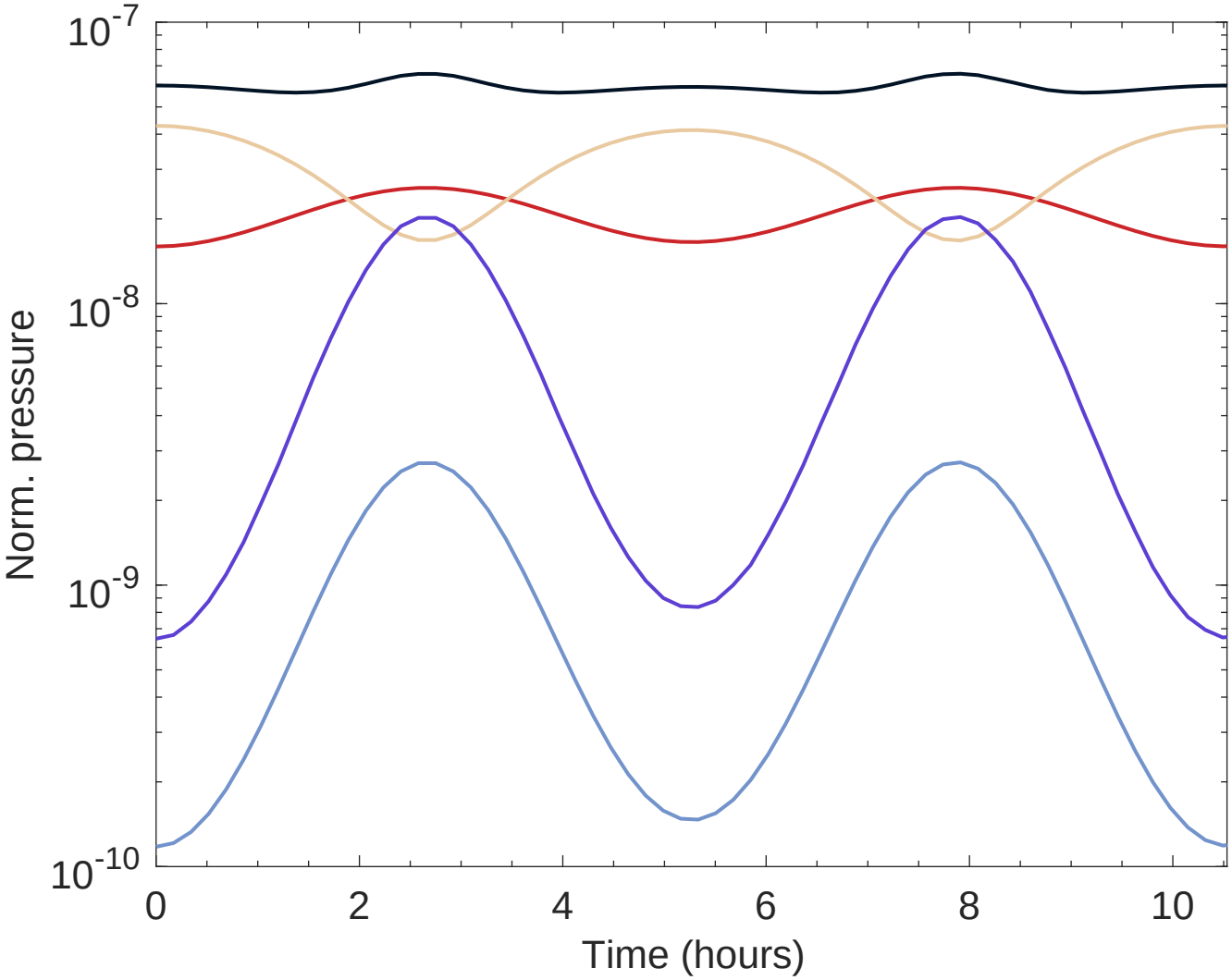
10^{-7}
10^{-8}
10^{-9}
10^{-10}
Norm. pressure
0
2
4
6
8
10
Time (hours)

Figure 9.

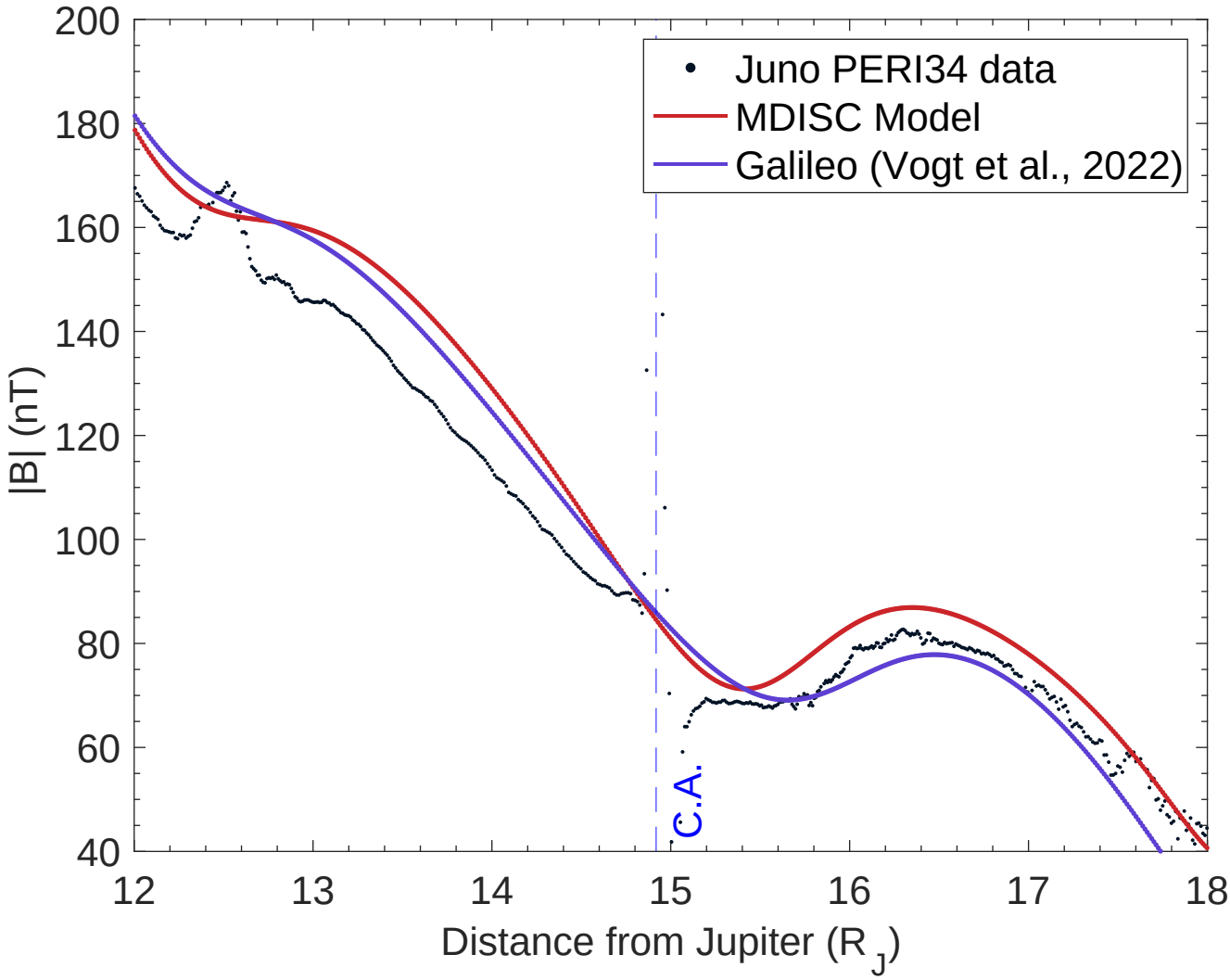
Juno PERI34 data
MDISC Model
Galileo (Vogt et al., 2022)
C.A.
|B| (nT)
Distance from Jupiter (R J)
200
180
160
140
120
100
80
60
40
12
13
14
15
16
17
18

Figure 9.

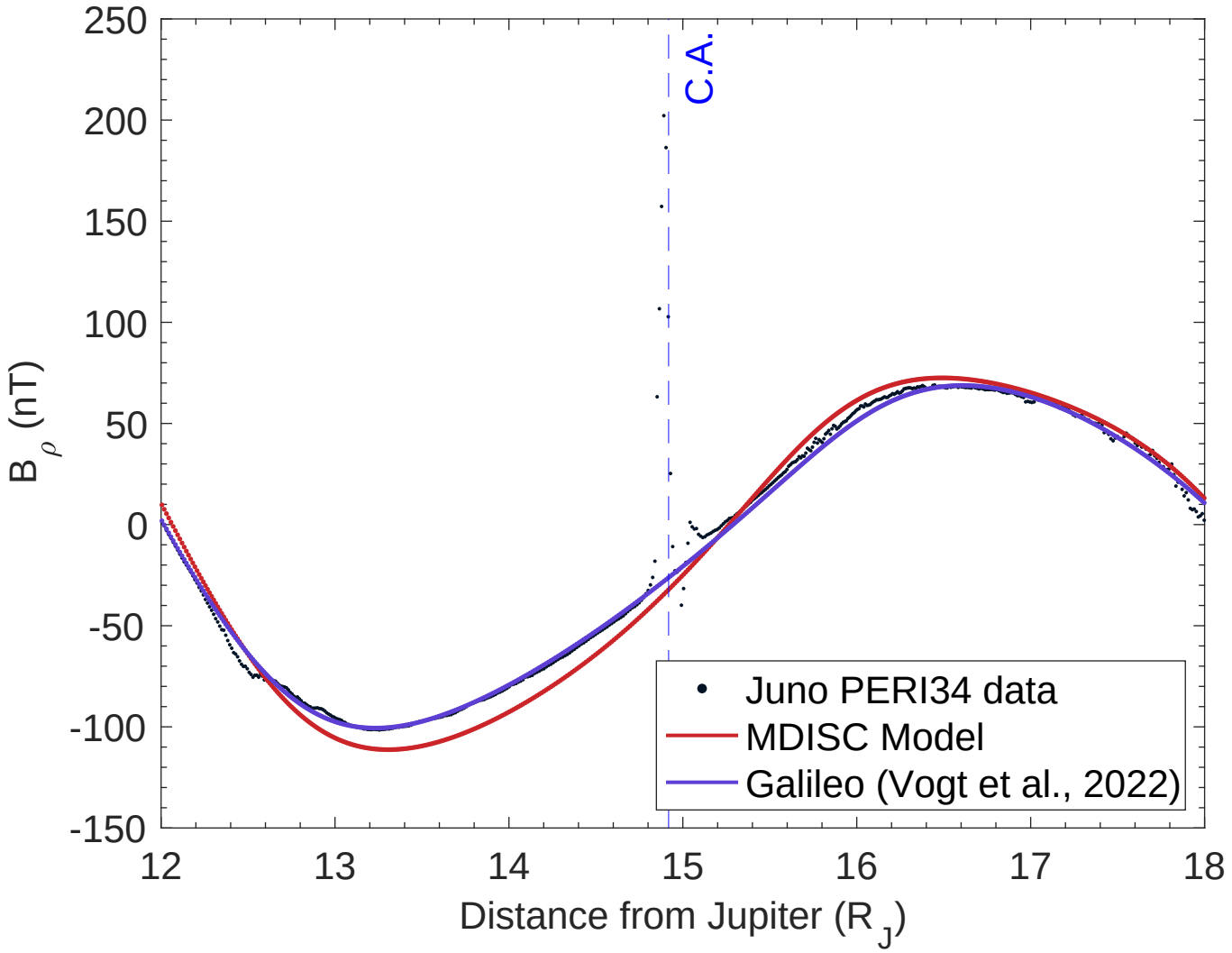
250
200
150
100
50
0
-50
-100
-150
12
13
14
15
16
17
18
B$_\rho$ (nT)
Distance from Jupiter (R$_J$)
C.A.
Juno PERI34 data
MDISC Model
Galileo (Vogt et al., 2022)

Figure 9.

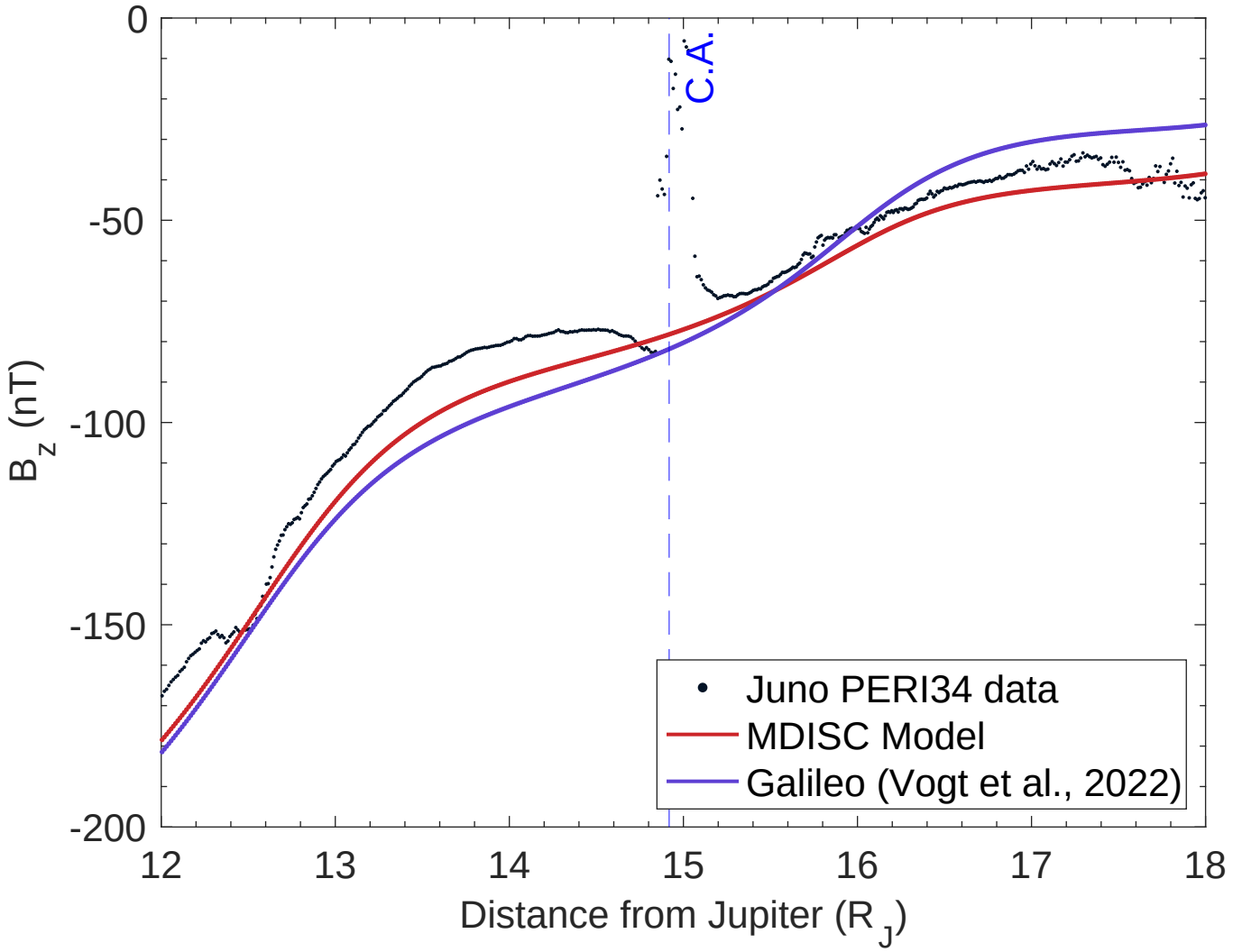
0
-50
-100
-150
-200
B_z (nT)
12
13
14
15
16
17
18
Distance from Jupiter (R_J)
C.A.
Juno PERI34 data
MDISC Model
Galileo (Vogt et al., 2022)

Figure 9.

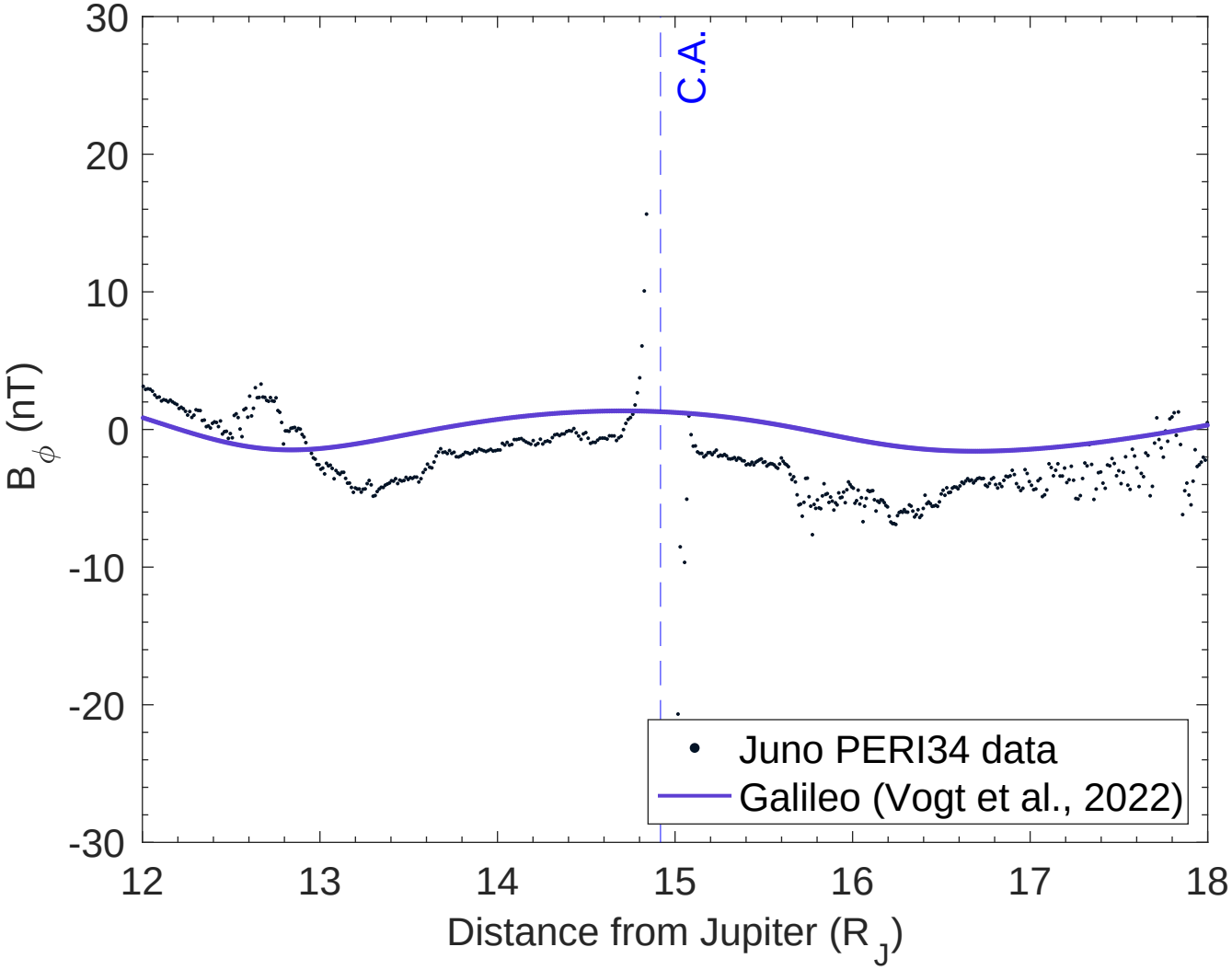
30
20
10
0
-10
-20
-30
12
13
14
15
16
17
18
C.A.
B_ϕ (nT)
Distance from Jupiter (R_J)
Juno PERI34 data
Galileo (Vogt et al., 2022)

Figure A1.

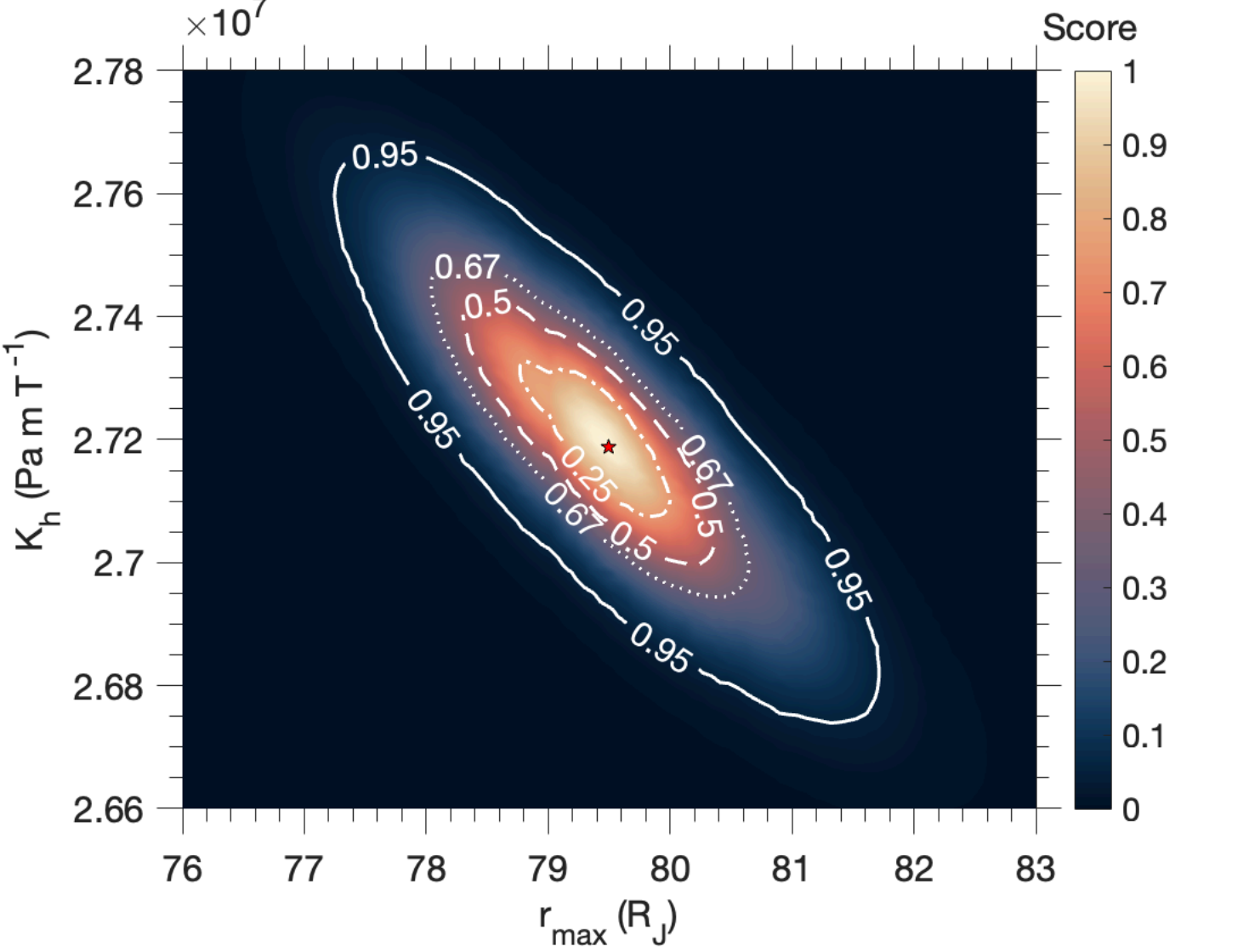
×10^7
Score
1
0.9
0.8
0.7
0.6
0.5
0.4
0.3
0.2
0.1
0
2.78
2.76
2.74
2.72
2.7
2.68
2.66
K_h (Pa m T^-1)
76
77
78
79
80
81
82
83
r_max (R_J)
0.95
0.67
0.5
0.25